APPLICATION OF WICKING FABRIC TO REDUCE DAMAGE IN ALASKAN PAVEMENTS

Final Project Report

By

Chuang Lin
Research Assistant

Xiong Zhang, Ph.D., P.E.
Associate Professor

Wendy Presler, M.S., P.E.
Research Assistant

Department of Civil and Environmental Engineering
University of Alaska Fairbanks

AUTC Project No. xxxxx
Project Title: Application of Wicking Fabric to Reduce Damage in Alaskan Pavements

Performed in cooperation with
TENCATE GEOSYNTHETICS (North America)
and
Alaska Department of Transportation & Public Facilities

December 2015

DISCLAIMER

The contents of this report reflect the views of the authors, who are responsible for the facts and the accuracy of the data presented herein. The contents do not necessarily reflect the official view or policies of the Alaska Department of Transportation & Public Facilities (AKDOT&PF). This report does not constitute a standard, specification or regulation.

ABSTRACT

Beaver Slide is located near kilometer 177.8 (mile 110.5) on the Dalton Highway. The road is sloped downhill when heading north. The road gradient is approximately 11%, and the road prism is on a side hill. Each year, soft spots usually appear in the pavement structure in late April and remain all summer. These soft spots have been called "frost boils". The "frost boils" have resulted in extremely unsafe driving conditions and frequent accident occurrences. Conventional repair methods have not worked. A newly developed geosynthetic wicking fabric was installed in the road structure in August 2010. The fabric has a high specific surface area (consequently high wettability and high capillary action) and high directional permittivity. Test results over the initial five-year period proved the effectiveness of the wicking fabric to mitigate "frost boils" and the subsequent road softening issue. Data collected during the past four years were analyzed to evaluate the long-term performance of the wicking fabric. A scanning electron microscope (SEM) was used to explore the interaction between the wicking fabric and in situ soils, and to determine the condition of the fabric five years after installation.

ACKNOWLEDGMENTS

The authors wish to express their appreciations to Tencate Geosynthetics (North America) for the funding and Alaska Department of Transportation & Public Facilities (AKDOT&PF) for their support that made this project possible. Appreciations also extend to Jeff Curry from AKDOT&PF and graduate student Lin Li and Chuang Lin whose efforts have contributed significantly to their works in in field and laboratory testing and data analysis for the project.

TABLE OF CONTENTS

Page

LIST OF FIGURES

Page

LIST OF TABLES

Page

CHAPTER I INTRODUCTION

Introduction and Background Information

Beaver Slide is near mile 110.5 on the Dalton Highway and it is downhill when heading north. The road gradient is approximately 11% and the road prism is on a sidehill. The embankment is about 4 feet on the high (southwest) side and 9 feet on the low (northeast) side. Each spring, there is shallow groundwater running downslope, and then coming up into the road embankment to cause frost boils and subsequent road damage (Figure 1(a)). The frost boils have resulted in extremely unsafe driving conditions and frequent accident occurrences. Past repair efforts indicate conventional road construction methods do not work.

The H2Ri Wicking Fabric has been newly developed by TENCATE GEOSYNTHETICS (North America). The fabric has a high specific surface area (consequently high wettability and high capillary action) and high permeability. Preliminary laboratory tests indicate it has great promise as a cost-effective mean to solve the frost-boil problems on northern road systems. In 2010, Alaska University Transportation Center, Alaska Department of Transportation and Public Facilities, and TENCATE GEOSYNTHETICS jointly funded a field implementation project to investigate the effectiveness of the H2Ri wicking fabric to mitigate frost boils in Alaskan pavements. A test section was constructed at a section of road with the most soft spots during 2010 spring break at the Beaver Slide from August 3-5, 2010. 22 pairs of moisture and temperature sensors were installed at different locations of the test sections to monitor the thermal moisture changes with time. Local climatic conditions such as hourly air relative humidity and temperature were also monitored. The test section has been monitored for about 2.5 years. Available data and field observations have clearly indicated that H2Ri wicking fabric has successfully eliminated the frost boil problem in the test section. Figure 1(b) shows the road conditions on May 24, 2011 (after the treatment).

The following conclusion was reached through the field monitoring of the performance of the H2Ri wicking fabric at the Beaver Slide test section as follows:

1. The obtained data indicated that there are two mechanisms for the “frost boils/soft spots” at the Beaver Slide: (a) frost heave and subsequent thaw weakening which occurred in early spring, and (b) upward pressurized water flow to road surface during lengthy rainy periods similar to artesian water.

2. The test section was built at an area with the most “soft spots” in the previous years. The same materials as those in the problematic zones were used for the construction of the test section, which reduced construction cost significantly. The test section has performed very well in the past 2.5 years. No soft spots or frost boils occurred in the test section treated with wicking fabric, while the soft spots or frost boils were observed during early springs or a particularly rainy period just beyond both the upper and lower ends of the test section in the past two years.

3. Changes in volumetric water content clearly indicated that the water was flowing along the direction of the wicking fabric to the shoulder of the pavement. Field observations indicated that the soil at the shoulder was damp.

4. Changes in volumetric water content and temperature in the pavement structure tended to indicate that the frost boils occurring in early spring were due to thaw-weakening only, since the soil above the ditch line was still frozen when frost boils appeared.

5. The wicking fabric successfully eliminated the frost heave and thaw weakening in the first 1.06 meters (3.5 feet) below the pavement surface (below the second layer of wicking fabric). The observed volumetric moisture contents indicated that the soils did not reach saturation in the test section. For the soils used in the Beaver Slide, it was an indication of no frost heave at all. However, for soils 4.5 feet below the center pavement surface, which was beyond the treated zone, there was an indication of excess water due to frost heave. However, it was too deep to cause damage the pavement structure.

6. The wicking fabric is an excellent material for draining water out of the pavement structure if properly used. The material itself has a high ability to absorb water from surrounding soils. It also has a high ability to transport water under differential water pressure. The pressure difference can be generated by exposing the wicking fabric to the atmosphere.

(a) Road conditions On May 12, 2010 (Before Treatment)

(b) Road conditions On May 24, 2011 (After Treatment)

Figure 1.1 Comparison of Road Conditions of the Beaver Slide at Different Times

Problem Statement

Although the test results are satisfactory, there is still concern whether the H2Ri wicking fabric can continuously perform well in the long run. It is worthwhile continuing the monitoring the performance of the H2Ri wicking fabric for a long time. With all the construction finished and sensors still functioning well, it is also cost-effective to conduct a long-term monitoring project.

Regarding the wicking fabric performance, there was concern that the clogging effect may influence the long-term performance of the wicking fabric. Because the wicking fabric was directly in contact with the soil, there was a potential that the drainage paths (or deep grooves) might become blocked by the fine particles in the soil. Additionally, there was concern that permanent deformation might influence the long-term performance of the wicking fabric. During the construction process, the soil above the wicking fabric was compacted and introduced relatively high loading pressure to the wicking fabric. The permanent deformation might be further developed with time due to heavy truck traffic on the road surface. Permanent deformation of the wicking fabric could reduce the amount of water held in the deep grooves and might reduce the effectiveness of the fabric's wicking ability. Researchers were also concerned that aging and mechanical failure could be major issues that influence the long-term performance of the wicking fabric. Both the hydrophobic and hydroscopic yarns of the wicking fabric would suffer from physical and chemical aging, but the rate of aging was uncertain. It is worthwhile to evaluate the effect of aging on the long-term performance of the fabric.

Research Objectives

The main objectives of this project are to 1) systematically monitor the moisture and temperature changes in the test section for a period of two years and three months including three spring breakups; 2) analyze the results together with the field visual observations to evaluate the long-term effectiveness of the H2Ri in reducing “soft spots” and improving performance of Alaskan pavements.

To achieve the objectives of this study, the following major tasks are proposed:

- Task 1: Field monitoring performance of the test section
- Task 2: Data processing and analyses
- Task 3: Draft of final report and recommendations

Research Methodology

To meet the objectives of this study, the following major tasks are accomplished:

- Task 1: Field monitoring of moisture and temperature changes and performance of the test and control sections

Soil-moisture contents and temperatures will be automatically measured at different depths at different locations of the test section through summer freeze/thaw annual cycles in a period of two years (January 2013 to February 2015). Hourly data measurements and storage will be made by the data-acquisition system. The research team will go to the site to collect data every four months to download data and make visual observations. Staff will also make visual observations from the Dalton Highway Maintenance & Operations (M&O) section of the AKDOT&PF.

- Task 2: Data Processing and Analyses

Results from the field monitoring of the moisture and thermal changes in the test section will be analyzed to identify the source and movements of water, as well as related "soft spots" mechanisms. The effectiveness of using the H2Ri wicking geotextile to prevent the "soft spots" in the long term will be evaluated.

- Task 3: Draft of Final Report and Recommendations

An interim and a final report will be drafted upon the completion of data analyses. The report will include a literature survey and investigation of the results of other researchers, the monitoring results, the findings of this research project, and suggestions for further study. The recommended uses of H2Ri wicking geotextile for further projects in Alaskan pavements will be provided as well.

.

CHAPTER II LITERATURE REVIEW

The soft spots were believed to be relevant to the formation of ice lenses in the soil and subsequent thaw weakening. As a result, one aim of the literature review focus is on previous studies on the use of geosynthetic materials to reduce ice formation and thaw weakening. Meanwhile, since the geotextile used in this project is relatively new, previous researches regarding the characterization of the geotextile are also investigated to grasp its basic hydraulic properties.

Mechanisms Causing Soft Spots

The three elements necessary for ice lenses to form, which may result in soft spots after thawing, are (Holtz and Kovacs 1981): 1) the presence of frost susceptible soil, 2) subfreezing temperatures, and 3) water supply from shallow groundwater table, infiltration, an aquifer, or held within the voids of fine-grained soils. All three of these conditions are met in many northern regions. Removal of any of the three conditions above eliminates, or at least minimizes, ice formation and thaw weakening. Numerous techniques have been developed to mitigate the damage to pavements and airfields caused by ice formation and thaw weakening.

Previously Developed Methods of Mitigating Ice Formation

The most common and widely employed technique is to remove the frost susceptible soils and replace them with non-frost susceptible soils. The non-frost susceptible soils are placed in layers thick enough to reduce the strain in the frost susceptible soil layers beneath to an acceptable level. This method is the removal of condition 1, above. To address this issue, AKDOT&PF stipulates that granular materials with fines content less than 6% must be used as base course material (AKDOT&PF 2004).

To remove condition 2 above, a common method is to include the use of insulation in the pavement section to reduce the freeze and thaw depth (Esch 1994). In many remote areas where the removal of frost susceptible soils and the reduction of subfreezing

temperatures are difficult and expensive, removal of available water could lead to savings in construction costs.

By breaking the capillary flow path, which will remove condition 3 above, ice formation will be less severe. A capillary barrier is a layer of coarse-grained soils or geosynthetic material that is placed in a frost susceptible soil to: 1) reduce upward capillary flow of soil water due to the suction gradient generated by evaporation or freezing, and (or) 2) reduce or prevent water from infiltrating from the overlying fine-pored, unsaturated soil into the soil below the capillary barrier (Henry and Holtz 2001). In the latter case, if the capillary barrier is sloped, the infiltrating water flows in the fine soil downwards along the interface with the capillary barrier. Granular capillary barriers have been used to successfully reduce ice formation in roads. Taber (1929) found that placing a layer of coarse sand above the water supply in frost-susceptible soil specimens being frozen from the top down eliminated ice formation. He also noted that ice formation requires substantially more water than is naturally available in the soil pores. Casagrande (1938) and Beskow (1946) described placing a layer of sand or gravel above the water table in road construction to reduce ice formation in overlying fine-grained soil. Later, Rengmark (1963) and Taivenen (1963) documented using a sand layer above the water table to help prevent ice formation in overlying frost susceptible soil.

Use of Geotextile Materials to Mitigate Ice Formation

In recent years, geotextiles and geocomposites were evaluated to determine their effectiveness, when used as capillary barriers, to reduce frost damage in pavement structures. Geosynthetic drainage nets have been found to serve as good capillary barriers under most conditions because of their large pore sizes. The performance of nonwoven geotextiles as a capillary barrier appears to be compromised by soil intrusion into their interiors, decreasing the pore size and increasing the affinity of the material to water. Hoover et al. (1981) and Allen et al. (1983) independently performed experiments indicating that certain geotextiles reduced ice formation when they were placed horizontally in upright, cylindrical soil specimens that were frozen from the top down with water freely available at the base. Henry (1988) noted the importance of the surface

properties of the geotextiles, i.e., that hydrophobic geotextiles were much more effective in reducing ice formation than hydrophilic geotextiles. Henry (1996) concluded that properly selected geotextiles reduce ice formation in soils by functioning as capillary barriers and summarized guidelines for granular capillary barriers. It was also concluded that in addition to serving as capillary barriers during freezing, and to reinforce or separate and filter subgrade layers, geotextiles probably can be used for a combination of functions to reduce frost-related damage during thaw.

Guthrie and Hermansson (2006) reported test results which indicated that unsaturated granular base material became saturated due to water vapor flow during freezing. Henry et al. (2002) proposed the use of a geocomposite capillary barrier drain (GCBD) as a promising method to reduce frost damage in pavement structures under unsaturated conditions. A GCBD consists of a capillary barrier layer sandwiched between transport layers. The function of the capillary barrier layer is to impede unsaturated flow, either upward or downward. The GCBD is similar to drains commonly used to minimize the impacts of frost. However, conventional drainage systems are not wholly effective in reducing water-related problems in partially saturated soils (Beskow 1991), while soil above the ground water table is unsaturated, and ice formation occurs through the capillary rise of water. The GCBD is used to perform as a capillary break and as a drainage system that can suck water out of soil - that is, provide drainage while the soil is unsaturated. The key to the success of such a system is the use of a material with high wettability, which means it can absorb water from unsaturated soils, and high permittivity, which means it can transport the absorbed water out of the pavement structure quickly. The transport layer used in Henry et al. (2002) was a very heavy, woven, multifilament material with a mass per unit area of 2,370 grams per square meter, a thickness of 3.2 millimeters, and an O95 size of 0.075 millimeters. The infiltration test results indicated that the use of the GCBD to limit moisture changes in pavement subgrades and bases was very promising. Furthermore, the GCBD prevented the moistening of the subgrade at many of the infiltration rates tested. Whether the capillary barrier will reduce or prevent ice formation by preventing upward flow during freezing was not tested.

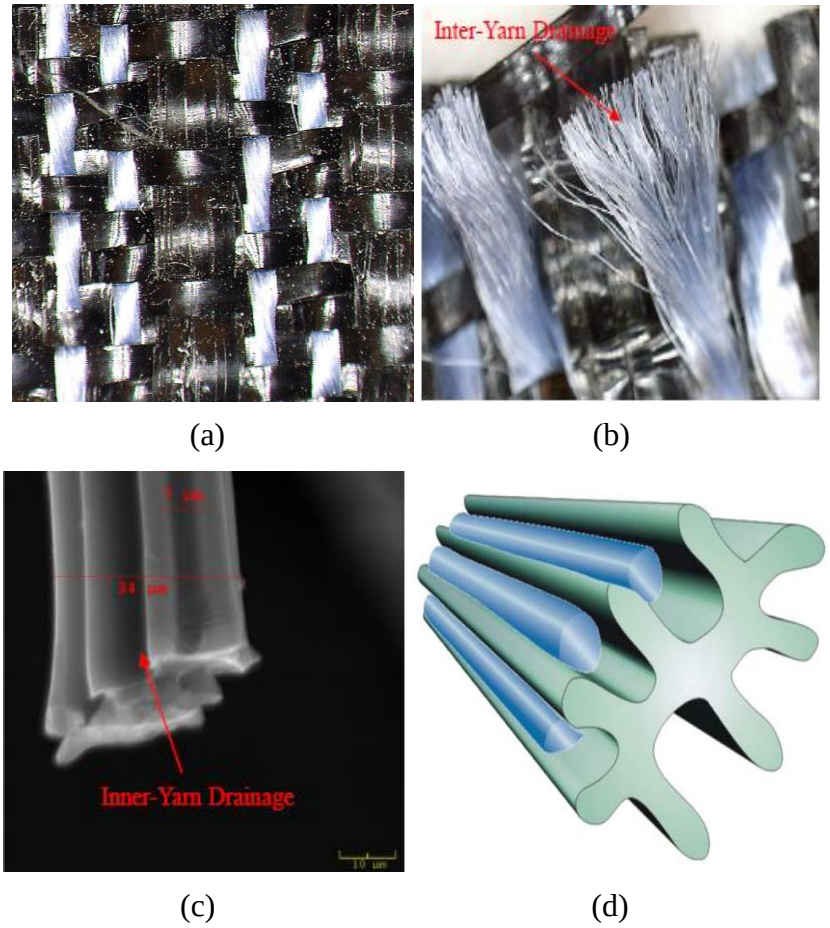

(a) (b)

(c) (d)

Figure 2.1 Wicking Fabric 2-layer Weave

A recently developed type of wicking fabric is made of nylon yarns and polypropylene yarns as shown in Figure 2(a). The black polypropylene yarns tend to repel water and have high tensile strength, which provide reinforcement and confinement options. The special hydrophilic and hygroscopic 4DG™ yarn (white yarn) has a high specific surface area (consequently high wettability and high capillary action) and a high permittivity, as shown in Figure 2.1(b). A microscopic image of the 4DG™ fiber (Figure 2.1(c)) indicates that the average diameter of the wicking fabric is about 34 microns and the groove spacing is approximately 7 microns. The multichannel cross-section has one of the highest available shape factors and has the greatest number of channels per fiber, which give the wicking fabric great potential for maximizing capillary action and water transport in an unsaturated environment, as shown in Figure 2.1(d). The specific surface

area of the wicking fabric is 3,650 square centimeters per gram, and it has a permittivity of 0.24 per second, which is equivalent to a flow rate of 611 liters per minute per square meter.

Table 2.1 presents the technical data sheet information for the wicking fabric. Zhang and Belmont (2009) performed a series of laboratory tests to investigate the performance of the wicking fabric to mitigate the frost heave and thaw-weakening problems in Alaska's harsh climate. The test results generally showed that the wicking fabric could potentially be used as a capillary barrier to mitigate frost heave. Although the results on the frost heave test were inconclusive, there were some definitive results indicating that the wicking fabric transports water under unsaturated conditions.

Table 2.1 Technical Data for Wicking Fabric

Mechanical Properties	Test Method	Unit	Minimum Average Roll Value	
			MD	CD
Tensile Strength (at ultimate)	ASTM D4595	lbs/in (kN/m)	450 (78.8)	450 (78.8)
Tensile Strength (at 2% strain)	ASTM D4595	lbs/in (kN/m)	45 (7.9)	75 (13.1)
Tensile Strength (at 5% strain)	ASTM D4595	lbs/in (kN/m)	135 (23.6)	325 (56.9)
CBR Puncture Strength	ASTM D6241	lbs (N)	2300 (10235)	
Permittivity	ASTM D4491	sec^{-1}	0.24	
Pore Size (O_{50})	ASTM D6767	microns	85	
Pore Size (O_{95})	ASTM D6767	microns	195	
Apparent Opening Size (AOS)[1]	ASTM D4751	U.S.Sieve (mm)	40 (0.43)	
Flow Rate	ASTM D4491	$gal/min/ft^2$ ($L/min/m^2$)	15 (611)	
Wet Front Movement[2] (24 minutes)	ASTM C1559[3]	inches	6.0 Vertical direction	
Wet Front Movement[2] (983 minutes) Zero Gradient	ASTM C1559[3]	inches	73.3 Horizontal direction	

[1]ASTM D4751: AOS is a maximum opening diameter value
[2]At standard temperature and pressure
[3]Modified

Previous Characterization of Geotextile

Zhang and Presler (2012) at University of Alaska Fairbanks conducted some fundamental tests regarding the hydraulic behavior of the wicking fabric. Figure 2.2 shows a laboratory test performed on the wicking fabric demonstrating the ability to absorb and transport water along the horizontal direction at a zero hydraulic gradient. In 983 minutes, the wetting front of the water moves 1.86 meters (73.3 inches) horizontally.

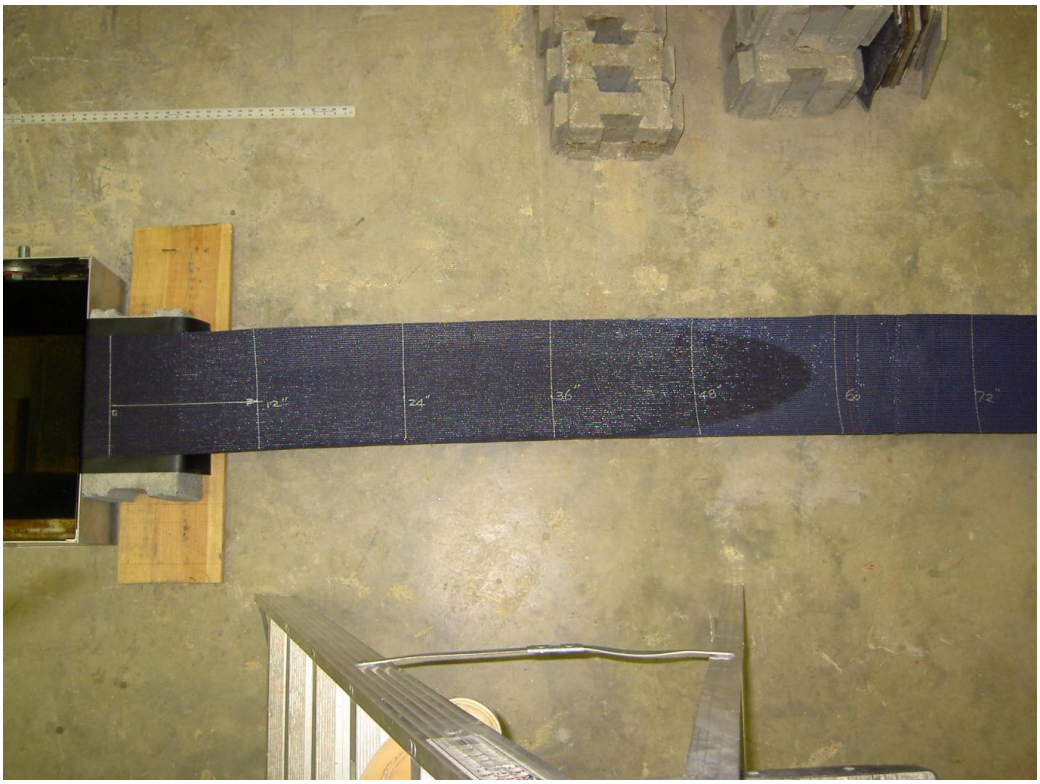

Figure 2.2 Water Movement in Fabric at Zero Hydraulic Gradient

Lin and Zhang (2015) also characterized the geotextile – water characteristic curve (GWCC). GWCC depicts the water content change due to suction variation. Basically, two types of tests are commonly used to determine the curve, including pressure plate test (to measure suction < 1500 kPa) and salt concentration test (to measure suction > 1500 kPa). The pressure plate testing equipment is shown in Figure 2.3(a). The pressure plate extractor drains the water out of the fabric by air pressure. Good contact between the fabric and porous stone should be maintained throughout the test. Therefore, a layer of soil slurry was used to ensure a good contact. At equilibrium condition, the geotextile water content was measured and the applied pressure was recorded. By conducting

several replications under different pressures, the geotextile – water characteristic curve within low suction range (< 1500 kPa) can be obtained.

Salt concentration test can be used to determine the relationship between water content and suction at high suction range (> 1500 kPa), as shown in Figure 2.3(b). The osmotic suctions of different electrolyte solutions were adopted to calibrate the relationship between suction and water content of the geotextile. Small pieces of geotextile were first saturated before putting into the desiccator. Then the saturated geotextiles were put into the container and the desiccator was sealed with tape. A period of 7 days is necessary to ensure the electrolyte solution and the geotextile were in equilibrium condition. After that, the water content was measured and the corresponding suction value was recorded.

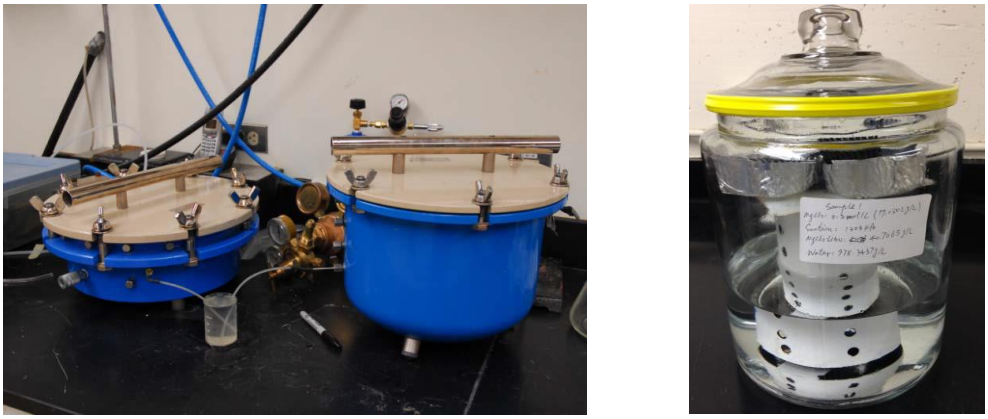

(a) Pressure Plate Test (b) Salt Concentration Test

Figure 2.3 Pressure Plate and Salt Concentration Tests Equipment

Figure 2.4 shows the GWCC test results in semi-log scale. There are several critical points need to be pointed out first. The air entry value is the matric suction at which air starts to enter the pores in geotextile. And the residual water content is defined as the large suction is needed to remove the additional water out of the geotextile. From the figure, the saturated water contents for the geotextile were approximately 30% - 35%. There are two types of drainage paths: inter-yarn drainage path and inner-yarn drainage path. Inter-yarn drainage path represents the drainage capability between fabric yarns and inner-yarn drainage path depicts the drainage capability within the multi-channel of each fiber. A simple regression curve similar is not adequate enough to demonstrate the

relationship between water content and suction for geotextile. One can expect that the GWCC consists of two components: one curve describes the combined effect of both inner-yarn and inter-yarn effect. When suction value has reached the inter-yarn air entry value (5-6 kPa) the inter-yarn stops working as a drainage material. Starting from this point, the inner-yarn or the wicking fabric dominates the shape of GWCC till suction reaches the inner-yarn air entry value (200 kPa). Following this assumption, the GWCC curve can be expressed as follows based on van Genuchten's (1980) equation:

$$w = 0.30 \times \left[\frac{1}{ln\left[2.718+\left(\frac{s}{6.653}\right)^{2.837}\right]}\right]^{1.006} \quad \text{(Suction < 45 kPa)}$$

$$w = 0.30 \times \left[\frac{1}{ln\left[2.718+\left(\frac{s}{254.056}\right)^{1.732}\right]}\right]^{1.174} \quad \text{(Suction > 45 kPa)}$$

Where,

w = water content; and

s = suction

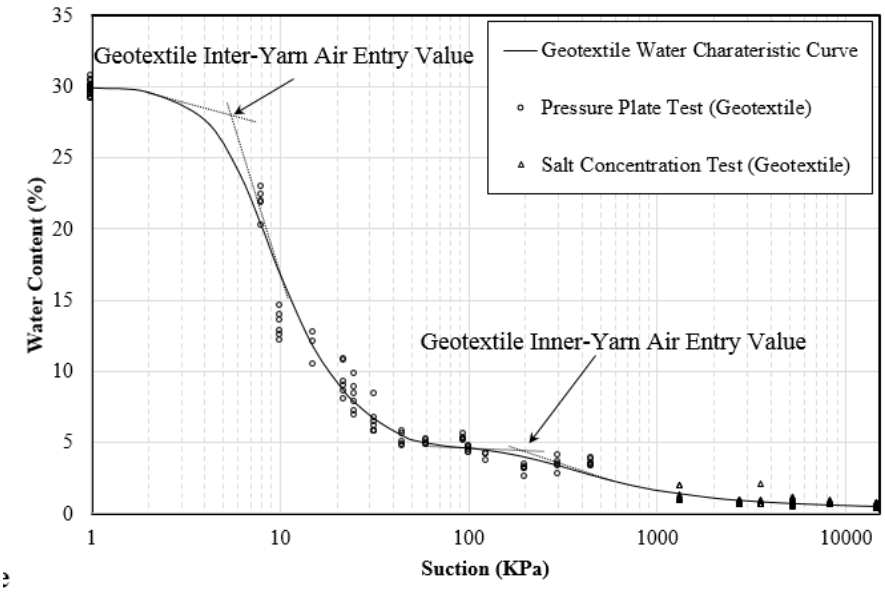

Figure 2.4 Geotextile Water Characteristic Curve

CHAPTER III CONSTRUCTION OF TEST SECTION AND INSTRUMENTATION

Even though the construction process has been introduced in the previous report (Zhang and Presler 2012), for the completeness and convenience for reference, the construction and instrumentation part is addressed and replicated in this section. This chapter consists of a description of the construction process at the test section, installation of instrumentation and data collection equipment, and observations of existing site conditions.

Construction Process

A test section of 18.1 meters (60 feet) was constructed at Beaver Slide from August 3, 2010 through August 5, 2010. The construction was performed according to the following procedure. The east (northbound) lane of the road was excavated to a depth of 1.06 meters (3.5 feet) below the original road surface, while the west (southbound) lane of the road was not excavated, to maintain the traffic flow, as shown in Figure 3.1.

Figure 1.1 Excavation of East Lane (Looking North)

Before installing the first layer of wicking fabric, three pits were excavated below the centerline, the edge of the original road, and the edge of the excavation limit, as shown in Figure 3.2 below. These pits were about 1.97 meters (6.5 feet) below the original road surface, or about 0.91 meters below the mass excavation level. At the bottom of the excavation pits, three pairs of sensors were installed and are numbered 13, 6, and 2, respectively. Each pair of sensors consists of a Campbell Scientific 107-L temperature sensor and a CS616-L water content reflectometer, as shown in Figure 3.3.

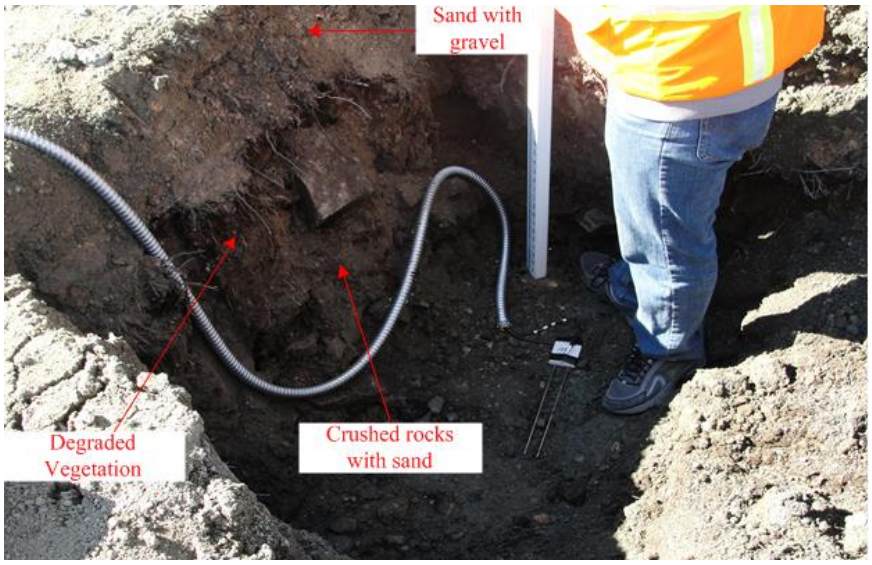

Figure 3.2 Excavation of Pit at Center of Road (Sensor 13)

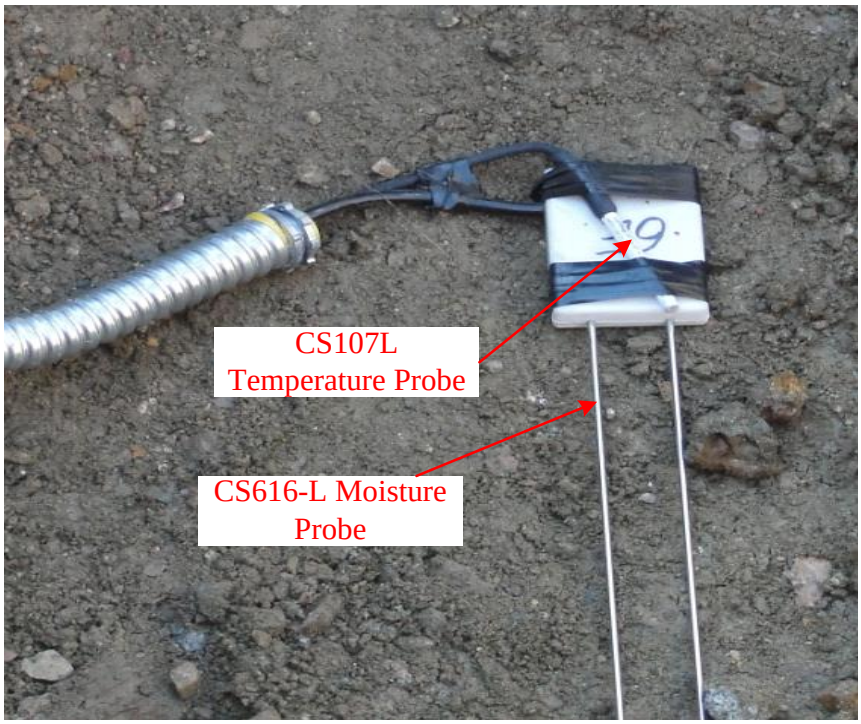

Figure 3.3 Temperature and Moisture Sensor

The excavation pits were then backfilled with soils originally taken out, and were compacted according to AKDOT&PF general construction procedures, as shown in Figure 3.4. Sensor pairs 1, 5, 9, and 12 were then carefully installed and the first layer of wicking fabric was installed. Since water transportation in the wicking fabric is directional, care was taken to make sure the direction of the wicking fabric was along the transverse direction of the road section, so that water in the road structure was transported horizontally to the road shoulder.

Figure 3.4 Bottom Layer of Wicking Fabric after Placement

The excavated soils were brought back to backfill the excavation area with a thickness of approximately one foot. The backfill was then graded and compacted on top of the wicking fabric. After the soils were compacted, sensors 4 and 8 were installed. Then a second layer of wicking fabric was installed. A portion of the two layers of wicking fabric is exposed to the air, about 1.21 meters (4 feet), at the road shoulder. After the second layer of wicking fabric was placed properly, the excavated soils were used to backfill the excavation area with a thickness of approximately one foot. The backfill was then graded and compacted, and then sensors 3 and 7 were installed. The rest of the soil was brought back to backfill the excavation in the east lane to its original elevation (Figure 3.5).

Figure 3.5 East Lane of Road after Construction

The next step in the construction process began with digging out the west (southbound) lane of the road to a depth of approximately 1.06 meters (3.5 feet), as shown in Figure 3.6. To avoid the possible introduction of water from the ditch into the road section, the west road shoulder was not excavated.

Figure 3.6 Excavation of West Lane of Road

After the bottom of the excavation was graded, a pit was then excavated at about 5.44 meters (18 feet) from the center of the road to install sensor 20. The excavation pit was backfilled, and sensors 16, 19 and 22 installed, followed by a layer of the wicking fabric, as shown in Figure 3.7. The same procedures as those described above were followed. The excavated soils were used to backfill the excavation area with a thickness of approximately 0.30 meters (one foot). The backfill was then graded and compacted. After the soils were compacted, sensors 11, 15, and 18 were installed. A second layer of wicking fabric was installed and the excavated soils were brought back to backfill the excavation area with a thickness of approximately another one foot.

Figure 3.7 First Layer of Wicking Fabric on West Side of Road

The backfill was then graded and compacted and then sensors 10, 14, and 17 were installed. After that, the rest of the soil was brought back to backfill the excavation to its original elevation. Approximately four feet of fabric was left exposed to the air on the east shoulder, the down-slope side of the embankment, where water will be allowed to drain out of the fabric and flow down the hill, as shown in Figure 3.8.

Figure 3.8 Covering Wicking Fabric with Crushed Rock at the East Shoulder

Instrumentation

As shown in Figure 3.9, all of the wires for the sensors were protected using aluminum conduit to prevent damage from the traffic loads. The aluminum conduits were grouped together, buried in a small ditch in the transverse direction, and connected to a Campbell Scientific CR1000 datalogger. In addition to the temperature and moisture sensors inside the test section, an HMP45C Air Temperature/Relative Humidity weather station was installed to monitor the air temperature and relative humidity at the test site. The panel temperature of the datalogger was monitored by the CR1000. All of the data acquisition devices were organized into an ENC14/16 -NC-NM weather-resistant enclosure, which was installed on the tundra on the west side of the road.

Figure 3.9 Construction of Data Collection Station

The locations of the sensors were surveyed using a Leica NA720. TBMW1 and TBMW2 presented in Figure 3.10 were temporary benchmark locations. In summary, 22 pairs of sensors were installed in the pavement structure. It is worthwhile to point out that sensor 22 was installed at the location closest to the drainage ditch, and can be used as a representation of the saturated moisture content in the pavement structure in summer time.

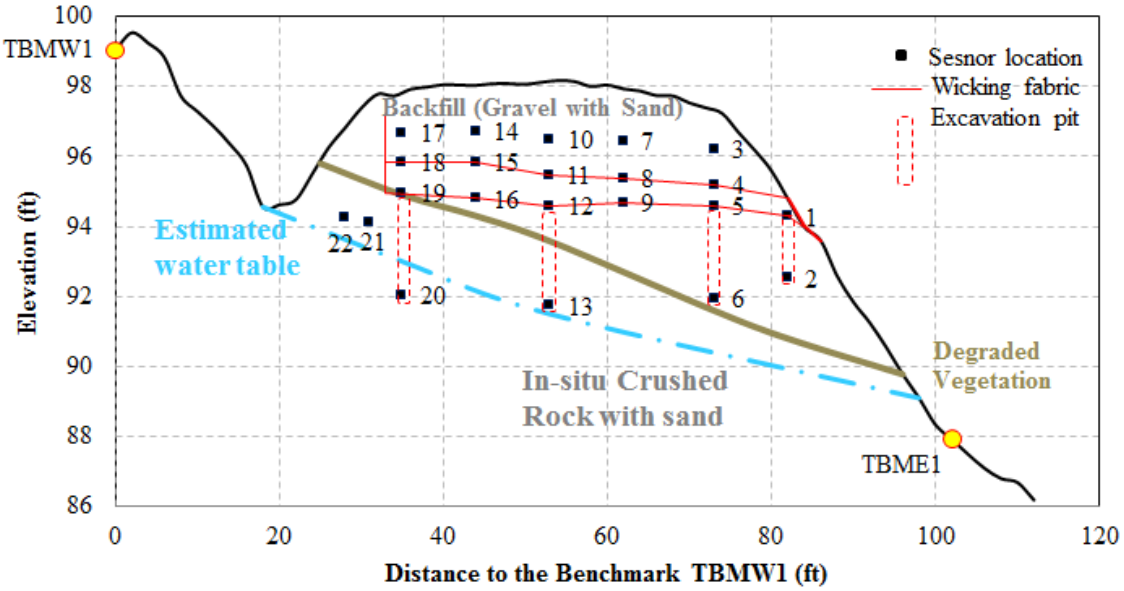

Figure 3.10 Sensor Locations, Groundwater and Soil Stratigraphy

Existing Site Conditions

Figure 3.10 shows the soil stratigraphy at the test section location, based upon the observations made during the construction process. It was found that the road section was built directly on the original tundra on the hill, using the degraded granite which was classified as silt with gravel, according to USCS classifications. Sieve analysis of the soils (Figure 3.11) indicated that some soils have fines contents greater than 6%, indicating that some soils at the site may be frost susceptible. Ground water was also encountered when installing sensor 20. Figure 3.10 above shows the approximate ground water table based upon these observations.

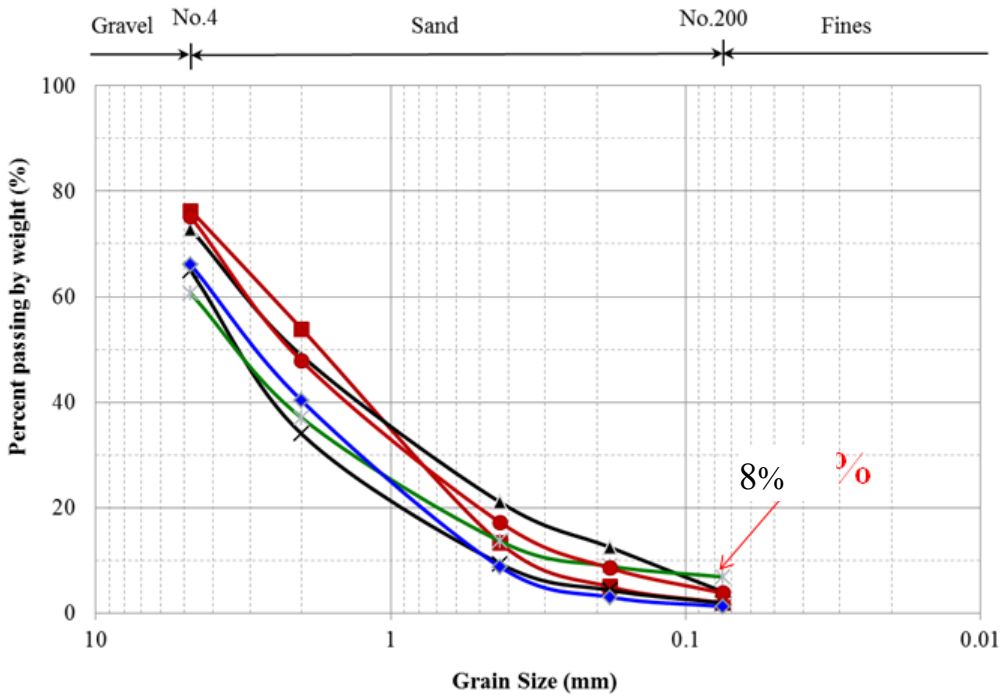

Figure 3.11 Sieve Analysis for Soils Obtained During Construction

The original tundra was encountered at about 0.91 meters (3.0 feet) below the ground surface at the west edge of the road, and at 1.36 meters (4.5 feet) below the surface at the centerline of the road section. It was about 2.72 meters (9 feet) lower than the road surface where it extended to the tree line at the west shoulder of the road. The buried vegetation encountered was degraded into a dark-yellow layer, which was about 0.05-0.1 meters (1-2 inches) thick. *In situ* crushed rocks with sand were encountered below the vegetation. Ground water was observed 0.15 meters (6 inches) below the tundra surface, once the tundra was removed. Additionally, standing water was observed during the construction process in the existing drainage ditch along the west side of the road. On the east side of the road, water was sporadically present along the tree line.

CHAPTER IV DATA DISCUSSION AND ANALYSIS

In this chapter, general climate conditions, soil temperature changes and soil moisture changes within the testing section are discussed. Since a previous paper has been published regarding the first two years wicking fabric performance, this chapter focuses on the overall performance during the entire monitored five years. Due to the malfunction of the data acquisition system, only four years data are presented here (from August 2010 to August 2014).

General Climatic Conditions

Figures 4.1 (a)–(b) present the hourly air temperature and relative humidity data, respectively, for the test section from August 2010 through August 2014.

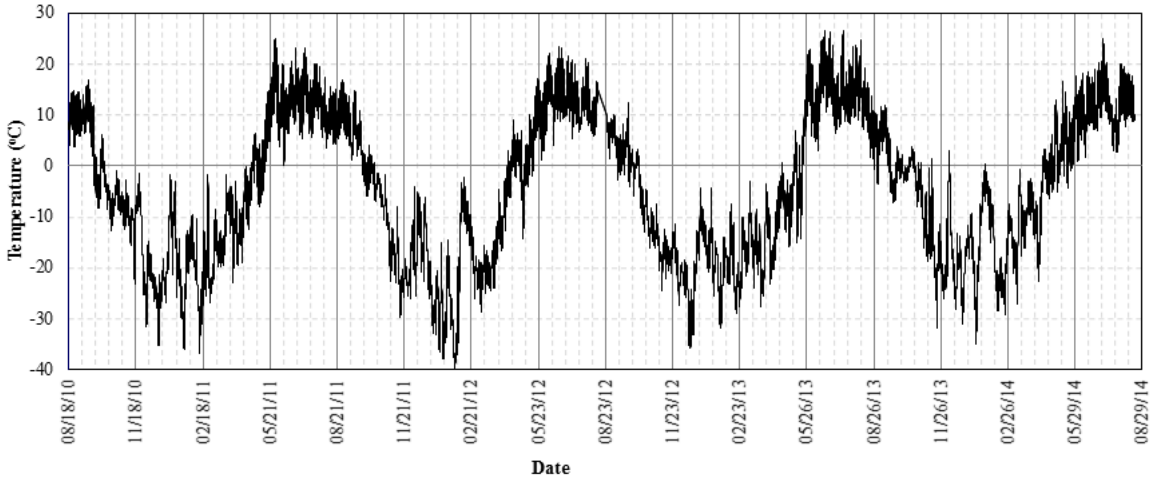

(a) Hourly Air Temperature Data

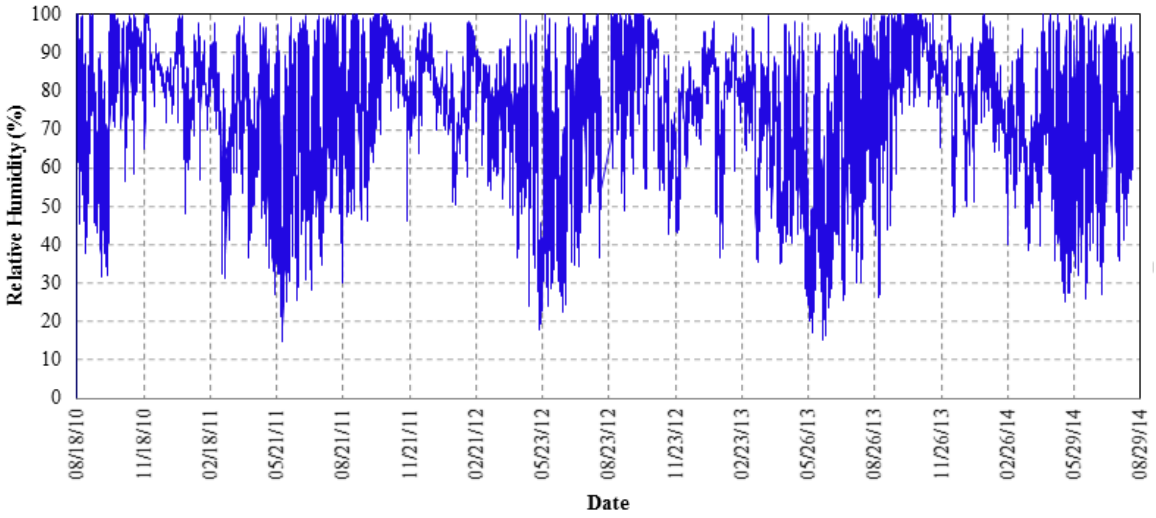

(b) Hourly Relative Humidity Data

Figure 4.1 Hourly Climatic Data at Beaver Slide Test Section

Figure 4.1(a) indicates that in general, the average summer air temperatures increased from 2011 to 2013, followed by a decrease in 2014. Each year, air temperatures dropped below zero in late September and rose above zero in mid to late April. The lowest temperatures recorded at the site each year were on February 23, 2010 (-36.8 °C), January 29, 2011 (-39.8 °C), December 17, 2012 (-35.2 °C) and January 13, 2014 (-34.8 °C). The highest temperatures recorded were on May 27, 2011 (24.4 °C), June 24, 2012 (22.9 °C), June 19, 2013 (26.2 °C) and July 6, 2014 (24.9 °C). The daily temperature variations in the summer time were smaller than those in winter times.

Figure 4.1(b) presents the monitored hourly relative humidity data for the four year period of August 2010 through August 2014. In winter months, the relative humidity at the site was between 70% and 90%, due to relatively low air temperature. However, the relative humidity varied from 20% to 90% in summer months. The relative humidity during daytime was lower than that at night. During significant rainfall events, the relative humidity increased rapidly to over 95% in the test section, and then decreased below 85% very soon after the rain stopped.

Soil Temperature Changes

Figure 4.2 presents the soil temperature at the 22 sensor locations from August 2010 through August 2014. Figure 4.2(a) shows the temperature variations for sensors 10, 11, 12 and 13, which were located at the center of the embankment. The sensors were buried at 0.45, 0.76, 1.06 and 1.97 meters (1.5, 2.5, 3.5, and 6.5 feet) below the road surface, respectively. In general, the trend of temperature changes in the soil followed the air temperature changes. The temperature changes in the soil decreased in magnitude as depth increased, due to the soil insulating effect. For instance, sensor 10 was located 0.45 meters (1.5 feet) below the surface, which was the closest sensor to the road surface, and its temperature variation followed the air temperature change very closely during the summer. During the winter months, the temperatures at sensor 10 were higher than the air temperatures, due to the insulating effect of snow on the road surface. In comparison, the temperature variation at sensor 13, which was installed 1.97 meters (6.5 feet) below the road surface, ranged from -12 °C to 3 °C for the entire year. The variation at sensor 13 was much smaller than that for the air temperature. It was also observed that the soil temperature 1.97 meters (6.5 feet) below the road surface only experienced temperatures above 0 °C for less than 3 months each year (i.e. July 20, 2012 to October 30, 2012). This indicates that the soil at 1.97 meters (6.5 feet) below the road surface could be considered as a permeable layer for approximately 3 months, while as an impermeable layer for the rest of the year.

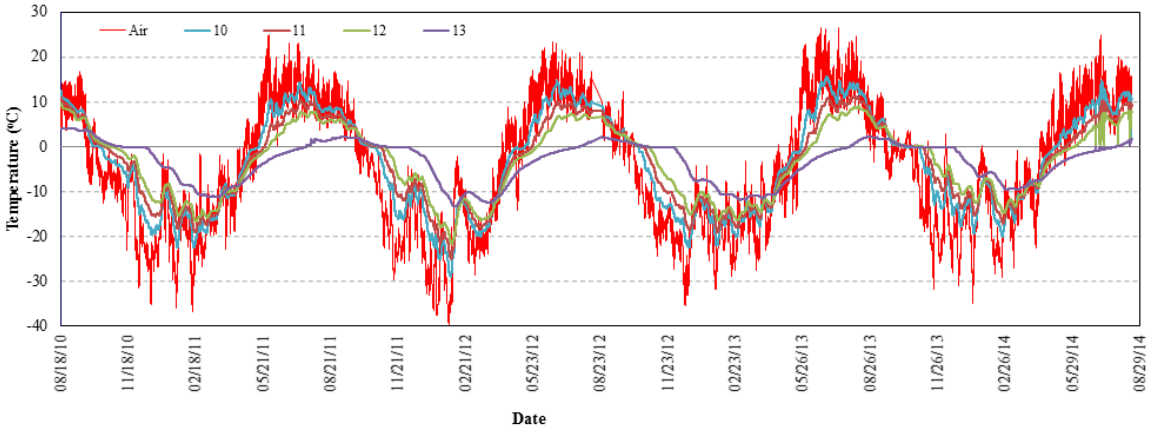

(a) Soil Temperature vs. Depth

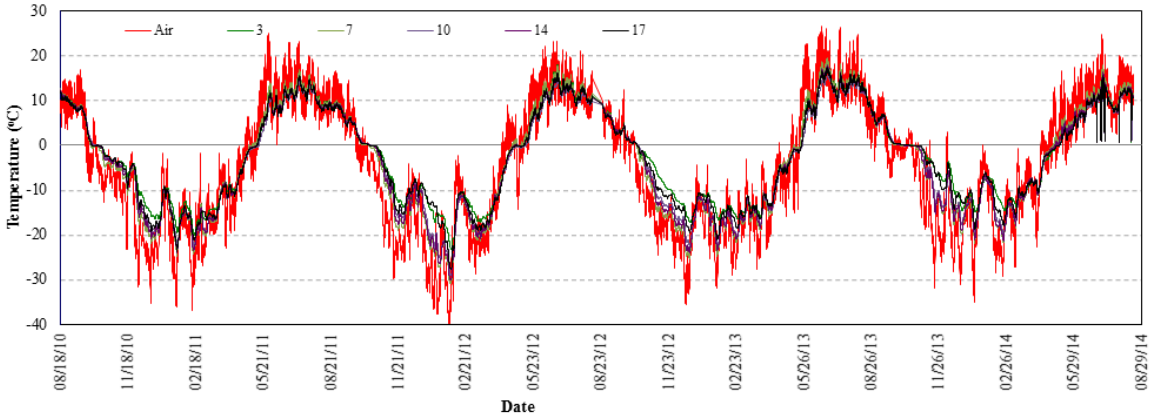

(b) 0.45 m below Road Surface

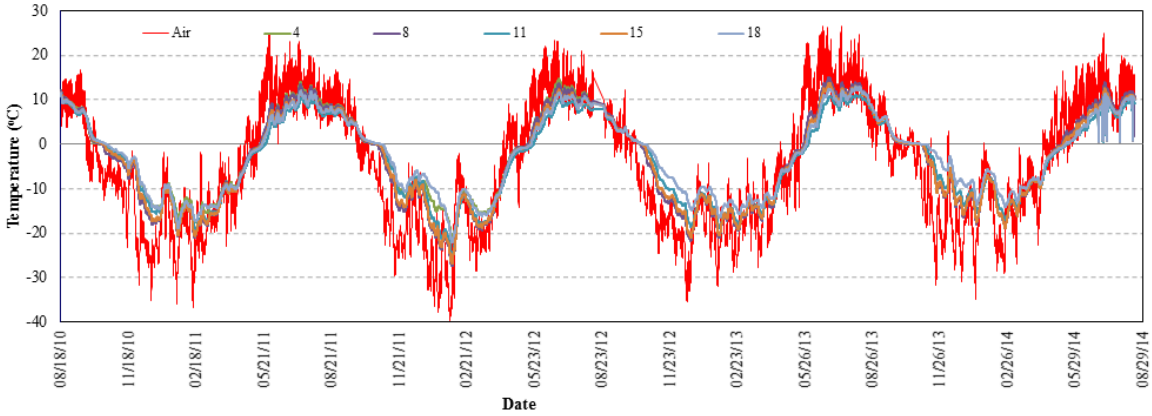

(c) 0.76 m below Road Surface

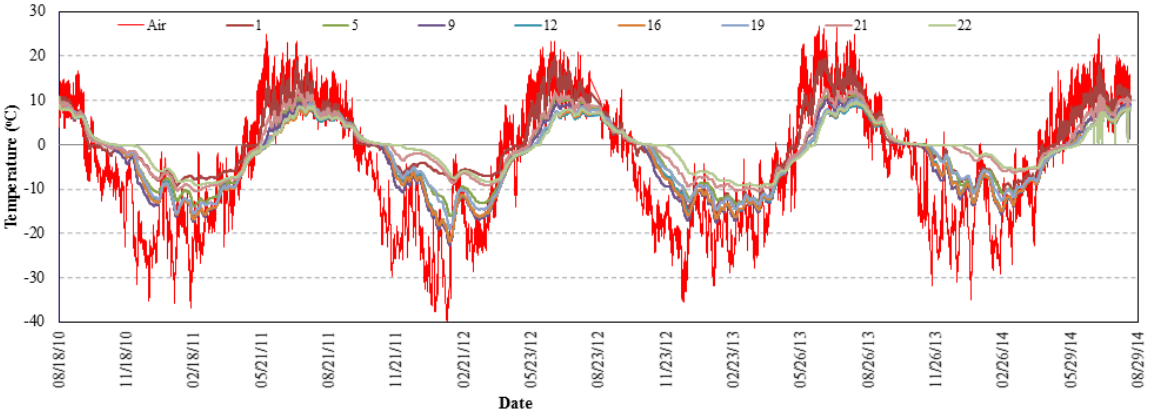

(d) 1.06 m below Road Surface

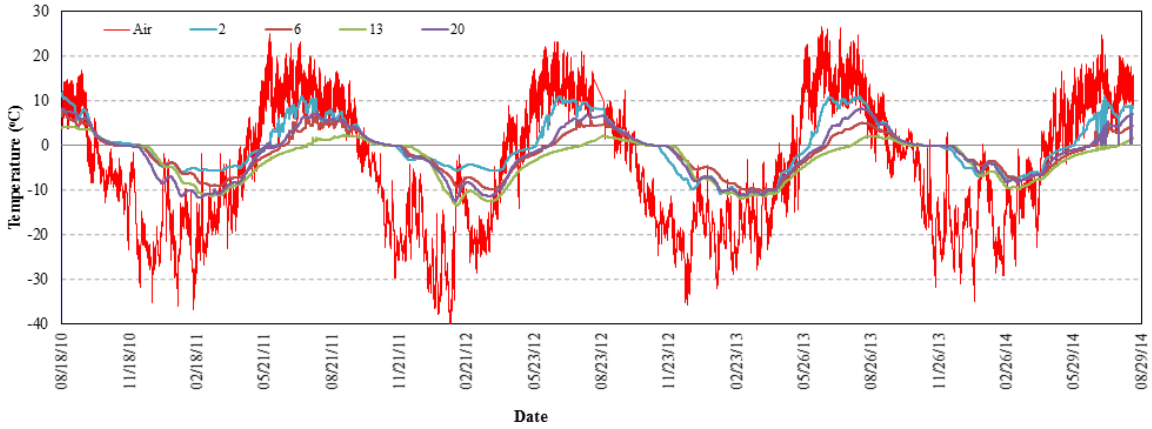

(e) 1.97 m below Road surface

Figure 4.2 Soil Temperature Changes

Figures 4.2 (b)-(e) show the temperature changes at the sensor locations 0.45, 0.76, 1.06 and 1.97 meters (1.5, 2.5, 3.5, and 6.5 feet) below the road surface for the past four years, respectively.

Figure 4.2 (b)–(c) present temperature changes for the sensors located at 0.45 meters and 0.76 meters (1.5 feet and 2.5 feet) below road surface. In general, the amplitudes of temperature changes at 0.76 meters (2.5 feet) meters were smaller than that at 0.45 meters (2.5 feet). However, the soil temperature changes in both layers followed the air temperature trend during the summer, and were warmer than the air temperature in winter months. Thus, soils 0.76 meters (2.5 feet) below the road surface could be considered as permeable layers during the summer and be able to drain the melting snow at the surface of the roadway. Additionally, the soil temperatures observed in the center of the road were lower than temperatures at the edges during winter months, and soil temperatures at the west side of the road were lower than those at the east side. There are two reasons to explain this phenomenon: (1) snow was routinely removed and piled on the shoulders, insulating the shoulders to make them warmer than the center of the road; and (2) the roadway on the east side received more solar energy than the west side, resulting higher temperatures at the east side of the roadway.

Figure 4.2 (d)-(e) shows the temperature changes for sensors at 1.06 meters (3.5 feet) and 1.97 meters (6.5 feet) below road surface. The insulation effect becomes more

obvious as depth below the surface increases. As can be seen in Figure 4.2(d), soil temperatures changes at 1.06 meters (3.5 feet) experienced approximately a 1 month time lag (time difference for the starting dates of soil and air temperatures above zero) compared with the air temperature changes. As for soils at a depth of 1.97 meters (6.5 feet), this time lag could be as large as three months, as shown in Figure 4.2(e). This phenomenon indicated that during the early spring (late April or early May), the soils at 1.06 meters (3.5 feet) and below were still frozen and could not be considered as a drainage layer until 1-3 months later. In other words, since the second layer of wicking fabric was installed at1.06 meters (3.5 feet) below the road surface, it would not be able to drain the water out of the embankment until early June. The first snowfall at the site is expected in early October each year, theoretically allowing the second layer of wicking fabric to remain functional till early November, when the soils at this depth become thoroughly frozen.

Soil Moisture Changes

Figure 4.3 shows the soil moisture changes for the installed 22 sensors during the four-year period from August 2010 through August 2014. As can be seen in Figure 3.10, sensor 22 was buried at about 1.2 meters (3.9 feet) below the road surface, and was 1.5 meters (4.9 feet) away from the up-slope drainage ditch. Its elevation was 0.1 meter (0.3 foot) below the drainage ditch. The drainage ditch had water flow all year around except during the winter when everything was frozen. The moisture content at sensor 22 was controlled by the drainage ditch and maintained saturated or nearly saturated. Therefore, it is reasonable to use sensor 22 as a reference for comparison purposes in all figures. As can be seen in Figure 4.3(a), moisture content at sensor 22 was relatively constant in the summers and winters between 2010 and 2014, and independent of the daily weather conditions. The recorded average volumetric moisture content continuously decreased from 0.38 in 2010 to about 0.32 in 2013, and slightly increased to 0.35 in 2014. However, the unfrozen water in winter months barely changed and was maintained within the range of about 0.07-0.12 when the soils were entirely frozen. It is also worth noting that it took nearly 2 months to thoroughly freeze the soil at this depth in winter months, but only took

about 2 weeks to thoroughly thaw the frozen soil in subsequent early spring. Taking the 2014 thawing season as an example, the unfrozen moisture content for sensor 22 was approximately 0.09 on April 10, 2014 when the average daily air temperature was -15.5 °C. However, this value increased to 0.14 on April 24, 2014, when the average daily air temperature changed to -1.1 °C. This phenomenon indicates that the unfrozen water content increases with an increase in the soil temperature in frozen soil even if the air temperature is still below zero.

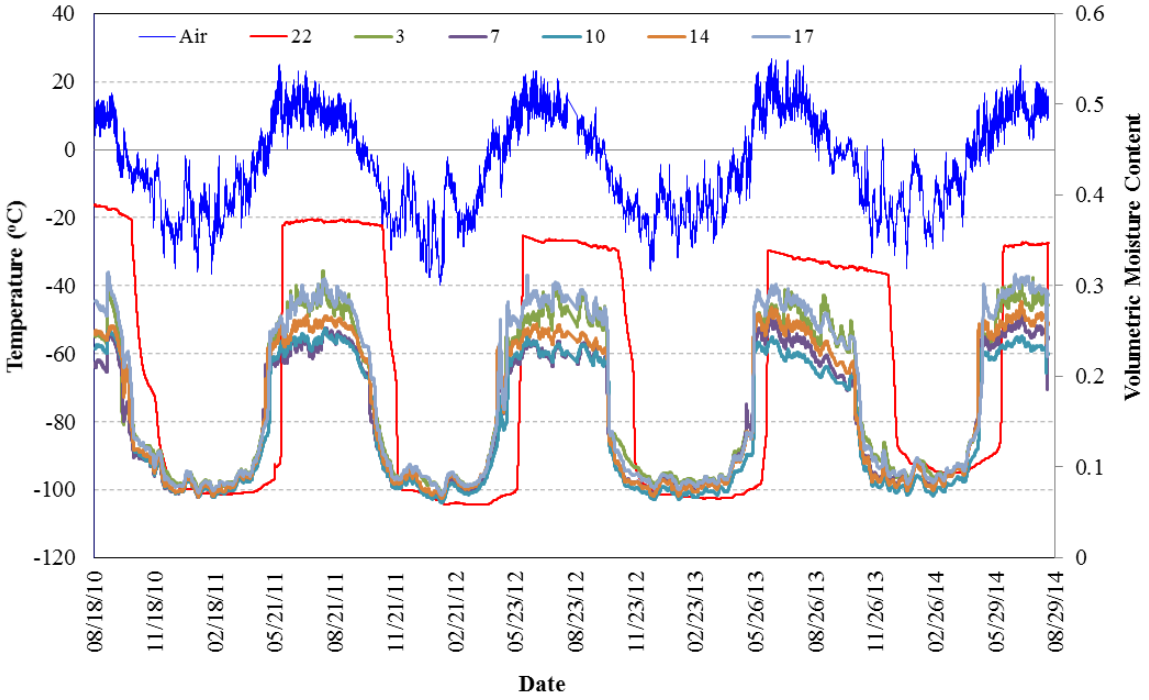

(a) 0.45 meters below Road Surface

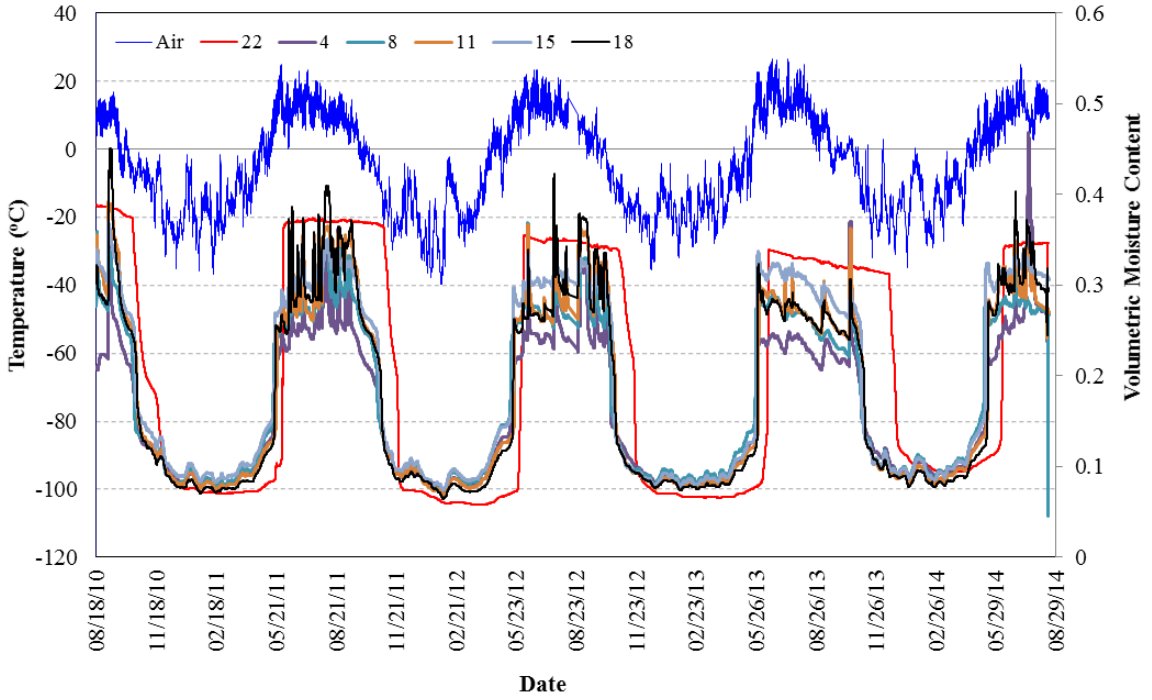

(b) 0.76 meters below Road Surface

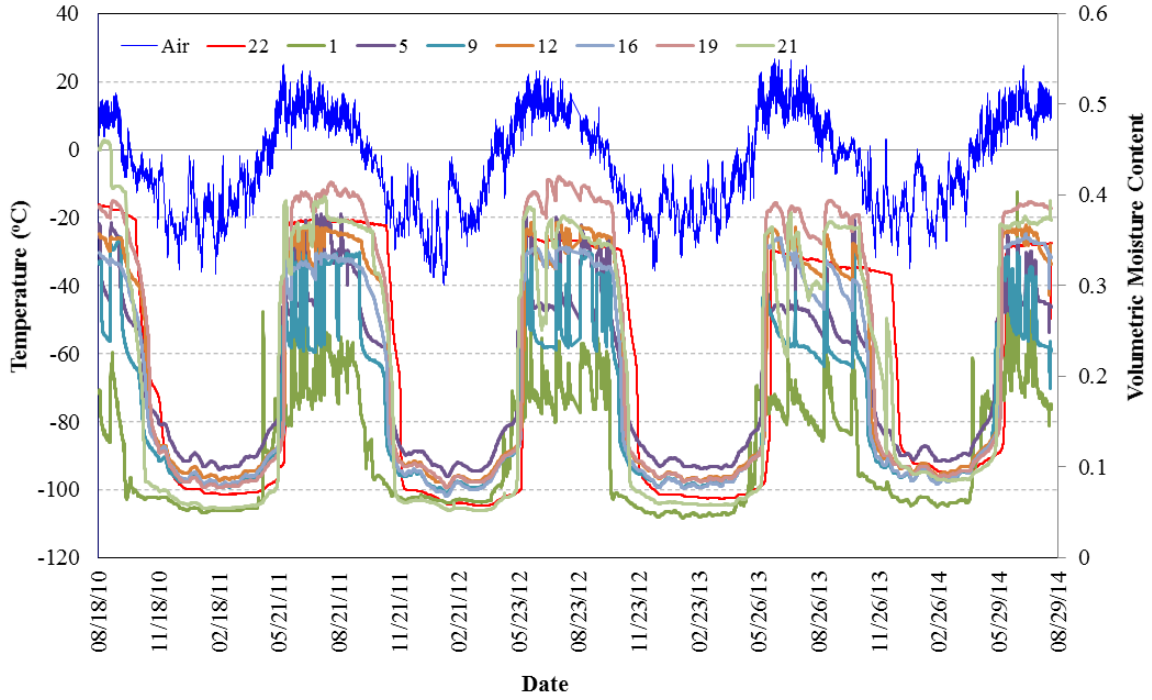

(c) 1.06 meters below Road Surface

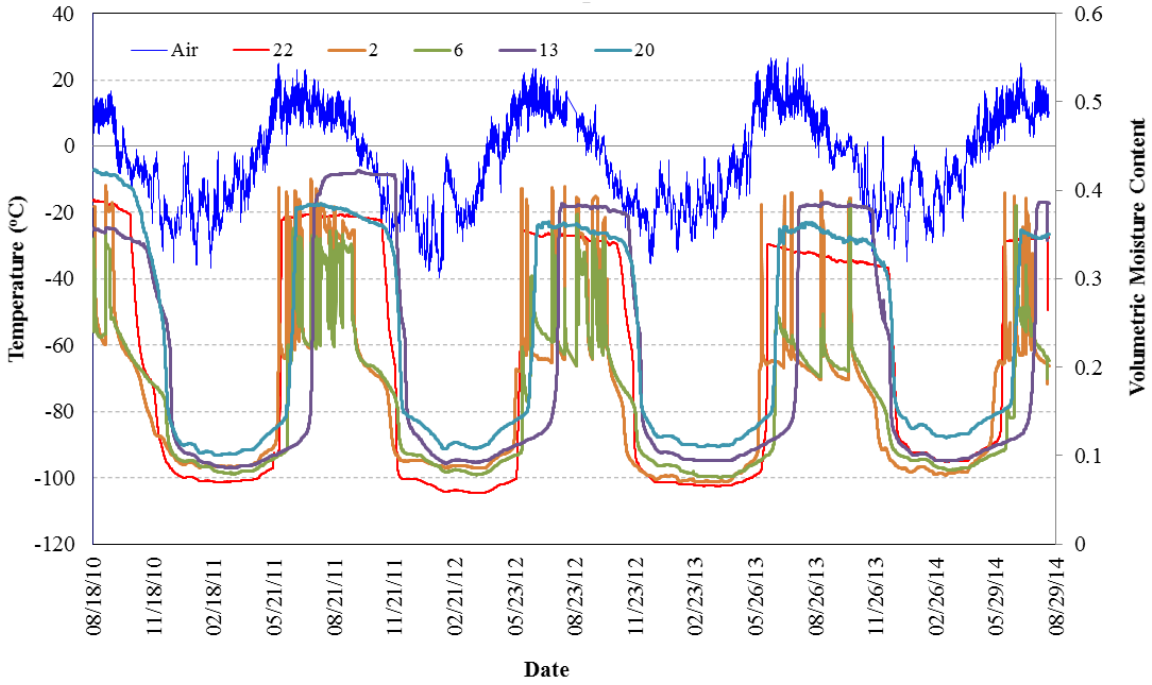

(d) 1.97 meters below Road Surface

Figure 4.3 Soil Moisture Changes

Figure 4.3(a) shows the soil moisture changes at 0.46 meters (1.5 feet) below road surface. It is obvious that the moisture contents at this depth were far below the moisture content at the reference location (sensor 22). This means that during the 4-year period, the soils always remained unsaturated. It is well known that when the soil moisture is low, its modulus and shear strength are significantly higher. Figure 4.3(a) is consistent with the observations made by AKDOT&PF maintenance and operation personnel who were very satisfied with the performance of the test section in the past five years. The test results indicated that the water from precipitation could be easily runoff due to the existence of both longitudinal and transverse slopes. Because the ground water table on west side was higher than on east side, and the frozen soil in the center of the pavement structure impeded the natural water flow, it is reasonable that the moisture contents of the soils on west side were higher (see moisture content at sensor 17).

Figure 4.3(b) shows the soil moisture changes for sensors at 0.76 meters (2.5 feet) below road surface, where the first layer of wicking fabric was installed. In general, the soil moisture contents were not higher than the reference moisture content at the location

of sensor 22, except for some long and intensive rainfall events. Any sudden, large variation in soil volumetric moisture content change indicated a rainfall event. Compared with Figure 4.3(a), soils at this depth, 0.76 meters (2.5 feet) were more affected by the rainfall events than soils at 0.46 meters (1.5 feet). However, the soil moisture contents dropped back quickly after the rainfall event stopped, which indicates that the drainage condition at this depth was favorable. Since the soils at 0.45m remained unsaturated in the four years as shown in Figure 4.3(a), the excessive water at the depth of 0.76m was from the horizontal direction.

Figure 4.3(c) shows soil moisture changes at 1.06 meters (3.5 feet) below road surface, where the second layer of wicking fabric was installed. Sensor 1 was buried fairly shallow on the east side of the road shoulder, and the moisture content was much lower than that for the reference sensor 22. Similarly, the moisture contents for sensors on the east side were all lower than at the location of the reference sensor, and the moisture content for sensors on the west side were all higher than at the location of the reference sensor. The amplitudes of moisture content changes after intensive rainfall events were also higher at 1.06 meters (3.5 feet) than at the previous two depths discussed. This phenomenon could be a result of (1) accumulated water at the drainage ditch, and (2) the one-month time lag to melt the frozen soil at this depth. Since the snow started to melt in late April, large amounts of water was trapped in the drainage ditch, which provided excess water to the roadway structure. Additionally, the temperature at the center line of the road was lower than that at the edges. Soil at 1.06 meters (3.5 feet) and below would not start to melt until late May or early June. The freezing temperatures and excess water resulted in a hard, frozen core at the center of the road, impeding the drainage path. Therefore, additional water was trapped in the area adjacent to and including the west side of the road, and resulted in higher moisture contents.

Figure 4.3(d) shows the moisture content changes for sensors at 1.97 meters (6.5 feet) below road surface. The moisture content distributions followed the trend presented in Figure 4.3(c). All of the sensors on west side had moisture contents higher than those on east side. It is noteworthy that sensor 13 (located at the centerline of the embankment) did not fully melt until mid-August, which is nearly 3 months after snow melting began.

As discussed previously, the frozen soil served as a hard core that impeded the natural water flow and caused excess water to become trapped on west side of the road. Moreover, because the melting process took such a long time, soils on the west side of the road embankment could hold more water during the summer time, allowing the unfrozen moisture contents to remain approximately 4% higher than the moisture contents at the reference sensor in winter months, and intensifying the frost heaving process. In contrast, the moisture contents for sensors on east side were much lower than at the reference sensor location, except for some intensive rainfall events.

Performance of Wicking Fabric at Different Climatic Conditions

The monitored hourly temperature and moisture data were used to establish temperature and moisture contour maps. The performance of the wicking fabric could be visualized via different climatic conditions: during rainfall events, during freezing process and during thawing process.

During Rainfall Events

Table 4.1 summarizes all of the major rainfall events for the four-year period monitored. Since the relative humidity in the air during the summer time is below 50% without rainfall, the water evaporation rate is faster than the precipitation water infiltration rate during light rainfall events. Moreover, the water can easily run off via the longitudinal and transverse slopes if the rainfall events are not intensive. Therefore, it is reasonable to assume that light rainfall events are not able to raise the relative humidity above 95%. Table 4.1 only summarizes the duration of rainfall events in which the recorded relative air humidity was greater than 95%. The total amount of rainfall hours were thoroughly recorded for three years: 530 hours in 2011, 617 hours in 2012 and 376 hours in 2013.

Table 4.1 Rainfall Events Summary

Year 2010			
Event	Date	Time	Duration (hrs)
1	8/18/2010	10	3
2	8/18/2010	23	12
3	8/23/2010	3	6
4	8/24/2010	3	7
5	8/24/2010	21	12
6	9/4/2010	15	23
7	9/6/2010	22	2
8	9/7/2010	11	23
9	9/9/2010	1	10
10	10/2/2010	15	1
Total Rainfall Hours			**99**

Year 2011			
Event	Date	Time	Duration (hrs)
1	5/23/2011	7	2
2	6/8/2011	21	8
3	6/9/2011	15	1
4	6/14/2011	7	4
5	6/15/2011	2	2
6	6/21/2011	2	11
7	6/22/2011	7	3
8	6/22/2011	12	3
9	6/22/2011	21	11
10	6/24/2011	0	6
11	6/26/2011	22	9
12	6/27/2011	22	2
13	6/28/2011	7	3
14	6/30/2011	3	6
15	6/30/2011	20	12
16	7/11/2011	20	39
17	7/16/2011	5	7
18	7/18/2011	5	7
19	7/24/2011	17	31
20	7/29/2011	19	43
21	8/1/2011	19	41
22	8/5/2011	0	4
23	8/5/2011	8	3
24	8/6/2011	0	2
25	8/7/2011	2	10
26	8/8/2011	1	8
27	8/10/2011	1	12
28	8/12/2011	3	4
29	8/13/2011	0	13
30	8/13/2011	20	15
31	8/20/2011	17	23
32	8/23/2011	21	16
33	9/1/2011	3	8
34	9/3/2011	5	8
35	9/3/2011	17	19
36	9/4/2011	23	1
37	9/6/2011	19	16
38	9/7/2011	20	19
39	9/8/2011	21	15
40	9/10/2011	9	29
41	9/12/2011	0	7
42	9/15/2011	20	10
43	9/16/2011	19	14
44	9/18/2011	1	23
Total Rainfall Hours			**530**

Year 2012			
Event	Date	Time	Duration (hrs)
1	5/13/2012	4	4
2	5/26/2012	6	27
3	5/29/2012	17	1
4	5/30/2012	1	2
5	6/2/2012	6	8
6	6/10/2012	1	12
7	6/27/2012	3	37
8	6/29/2012	6	28
9	7/4/2012	2	5
10	7/4/2012	19	11
11	7/17/2012	4	2
12	7/23/2012	4	8
13	7/24/2012	12	16
14	7/30/2012	23	8
15	8/2/2012	4	13
16	8/3/2012	9	6
17	8/4/2012	0	13
18	8/5/2012	0	8
19	8/6/2012	23	16
20	8/7/2012	22	5
21	8/25/2012	21	39
22	8/28/2012	0	3
23	8/29/2012	0	63
24	9/1/2012	7	30
25	9/3/2012	17	15
26	9/4/2012	23	11
27	9/5/2012	19	41
28	9/8/2012	0	14
29	9/15/2012	17	12
30	9/18/2012	13	27
31	9/23/2012	16	10
32	9/28/2012	20	60
33	10/2/2012	5	32
34	10/5/2012	7	30
Total Rainfall Hours			**617**

Year 2013			
Event	Date	Time	Duration (hrs)
1	6/4/2013	4	3
2	6/4/2013	12	1
3	6/4/2013	18	5
4	6/9/2013	22	6
5	7/1/2013	2	4
6	7/8/2013	3	4
7	7/8/2013	23	12
8	7/9/2013	23	15
9	7/16/2013	7	5
10	7/16/2013	20	12
11	7/18/2013	4	1
12	7/19/2013	15	20
13	7/20/2013	17	1
14	7/24/2013	20	1
15	7/30/2013	3	3
16	7/31/2013	6	2
17	8/5/2013	4	2
18	8/10/2013	18	9
19	8/12/2013	7	4
20	8/14/2013	11	3
21	8/14/2013	21	13
22	8/16/2013	4	6
23	8/18/2013	0	11
24	8/19/2013	19	15
25	8/21/2013	6	4
26	8/24/2013	3	1
27	8/28/2013	22	5
28	9/2/2013	18	16
29	9/3/2013	18	14
30	9/5/2013	17	15
31	9/7/2013	1	13
32	9/7/2013	20	4
33	9/9/2013	0	13
34	9/11/2013	22	10
35	9/11/2013	14	6
36	9/13/2013	20	9
37	10/13/2013	1	101
38	10/15/2013		
Total Rainfall Hours			**376**

Year 2014			
Event	Date	Time	Duration (hrs)
1	5/17/2014	13	4
2	5/22/2014	6	3
3	5/31/2014	19	38
4	6/5/2014	5	5
5	6/6/2014	13	17
6	6/9/2014	2	14
7	6/11/2014	0	14
8	6/11/2014	18	16
9	6/18/2014	1	7
10	6/19/2014	0	3
11	6/22/2014	4	9
12	6/25/2014	18	54
13	7/8/2014	1	13
14	7/8/2014	22	13
15	7/11/2014	12	15
16	7/15/2014	18	44
17	7/18/2014	23	10
18	7/19/2014	20	17
19	7/22/2014	5	31
20	7/23/2014	18	16
21	7/25/2014	2	9
22	8/1/2014	0	13
23	8/2/2014	0	9
24	8/7/2014	9	2
25	8/7/2014	15	1
26	8/14/2014	6	3
27	8/15/2014	13	43
Total Rainfall Hours			**423**

In a summary, the effect of rainfall intensity was limited due to the good drainage base course material (gravel with sand). Therefore, only the effect of rainfall duration is discussed in this section. Figure 4.4 shows the comparison of two rainfall events to demonstrate this effect: one is a short-term rainfall event lasting several hours, and the other is a relatively heavy rainfall event lasting for several days. As shown in Figure 4.4(a), the first recorded rainfall occurred at 10 pm on August 28, 2013 and lasted for 5 hours. By looking up the recorded data, it was determined that no other significant rainfall events occurred within a week prior to this rainfall event. The 3 moisture contour figures demonstrate the soil moisture distributions before the rainfall, 1 hour after the rainfall and 1day after the rainfall. It was apparent that the soil moisture distribution did not change significantly as a result of this event. This phenomenon indicated that a 5-hour rainfall was not long enough to change the water moisture distribution within the pavement structure. In comparison, another rainfall occurred at 11 pm on July 8, 2013 and continued on the following day. The total rainfall duration was about 27 hours from July 8 to July 9, ending around 2 pm on July 9. Figure 4.4(b) shows the soil moisture distribution at the beginning of the rainfall event, 7 hours after the rainfall and about 1 day after the rainfall. The soils in east side of the roadway were significantly drier than the soils on west side of the roadway prior to the rainfall. 7 hours after the rainfall event, more water had accumulated in both the east and west sides of the road structure. The saturation zone in the west side was larger because water flowed into the pavement structure via a drainage ditch up-slope and adjacent to the west side of the embankment. Meanwhile, on east side of the road, the saturated zone was observed at the location of the wicking fabric layers. This phenomenon indicated that the wicking fabric was able to suck the water from the surrounding soils and laterally transport it to the shoulder. The third contour figure shows that 1 day after the rainfall event, the saturation zone was smaller than before in the west side of the roadway. The soils near the wicking fabric were comparatively drier than the rest of the soils on east side of the embankment, where no apparent saturation zone was observed.

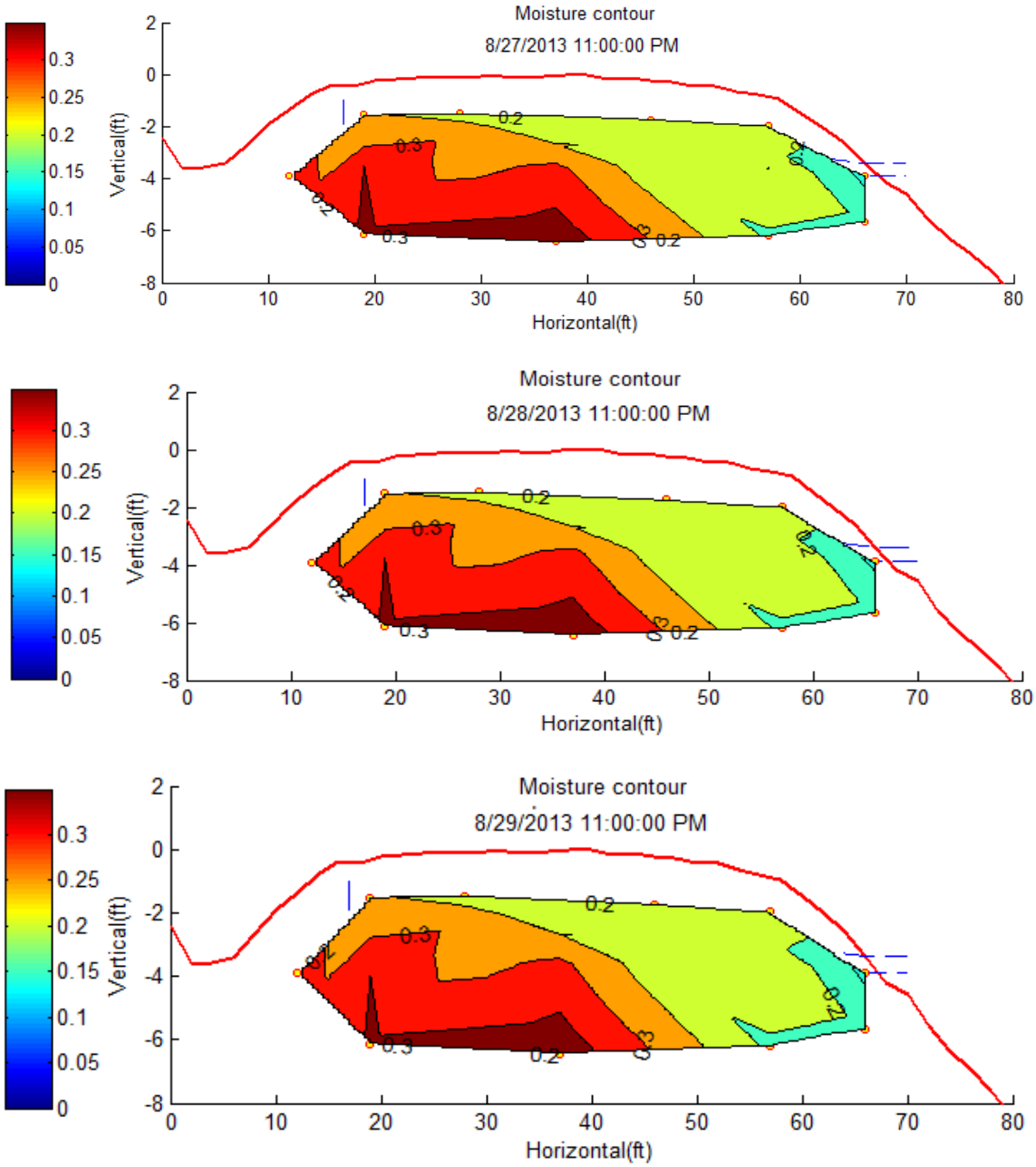

(a) Short Time Rainfall Events

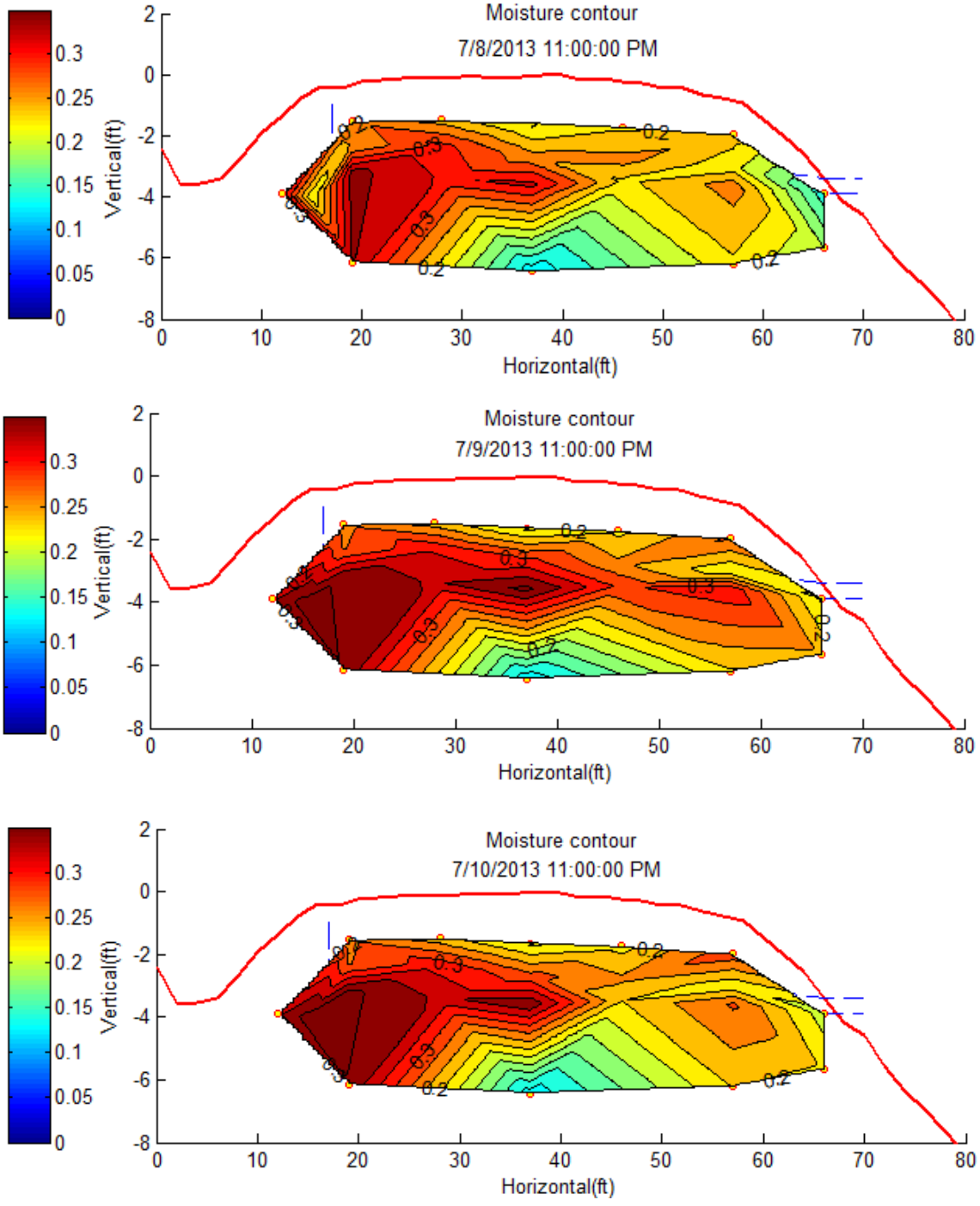

(b) Long Time Rainfall Event

Figure 4.4 Soil Moisture Contours during Rainfall Events

During Freezing Process

For purposes of this discussion, we focused on 2012 data in our analysis of the freezing process. The air temperature dropped below zero on October 4, 2012; however, the temperature in the soil was still above zero, as shown in Figure 4.5(a). It is critical to determine the moisture content distribution before the freezing front moves downward, because the water stored in the soil (both frozen and unfrozen) is the major factor influencing the severity of the "frost boiling" phenomenon in the subsequent spring. There were still two major saturation zones in the west side of the road; however, the moisture content in the east side was relatively low (about 0.2). This indicated that soft spots in the following spring, if frost boiling was observed, would be expected first in the west lane of the road surface. Also, it would take a much longer time for the freezing front to move downward in the west side, as shown in Figure 4.5(b). It was discovered (Zhang et al. 2014) that the freezing front (0 °C isothermal curve) nearly coincides with the location of the 0.2 volumetric water content curve. The freezing front extended to about 0.76 meters (2.5 feet) below the road surface on October 20, 2012 on west side, and to approximately 1.07 meters (3.5 feet) on east side. Moreover, the saturated zone was observed extending to the bottom sensor in the west side. Since the latent heat of water is relatively large compared with soil, it would take much more energy to freeze the soil on west side, where the moisture content was higher. Furthermore, the area exposed to the freezing air on east side was larger than on west side, so it is reasonable to assume that the freezing front moved faster on east side of the road. If this holds true, the wicking fabric would stop functioning in early October, due to the frozen drainage paths where the fabric is exposed to the freezing air on the east side of the road. Figure 4.5(c) shows that the entire pavement structure was frozen on December 3, 2012, which was about two month after the air temperature dropped below zero. The unfrzeon volumetric water content in the frozen soil was consisitent, averaging about 0.07.

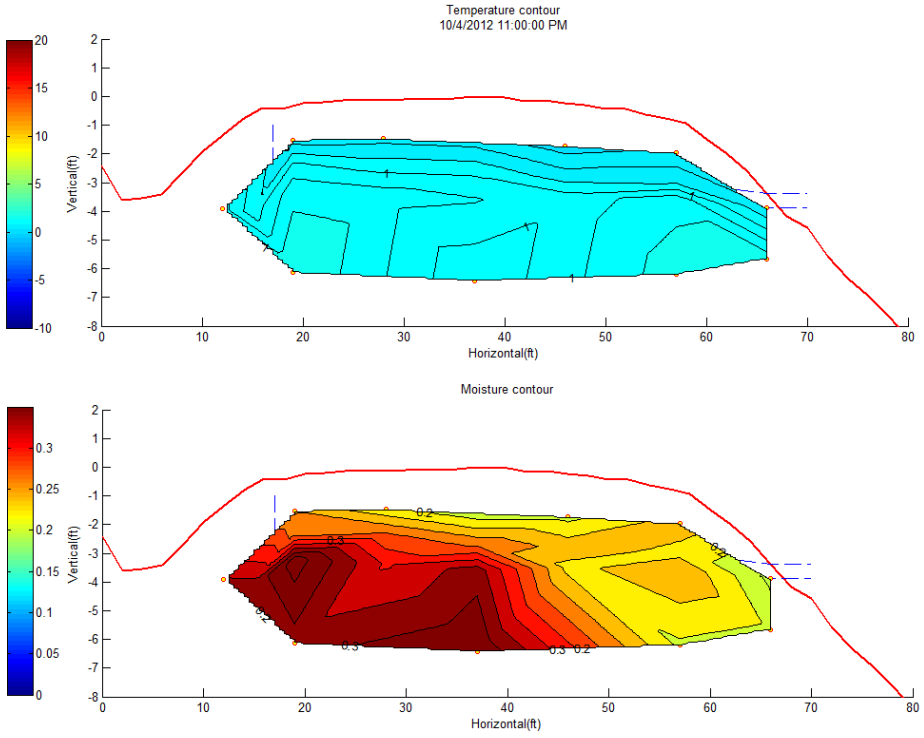

(a) Temperature and Moisture Contour on October 4, 2012

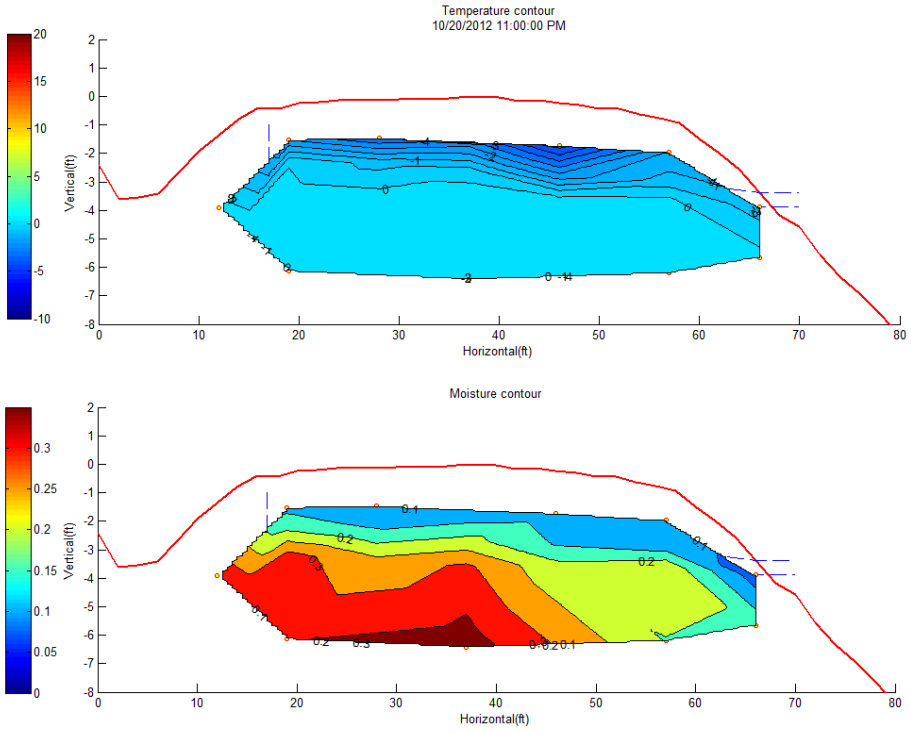

(b) Temperature and Moisture Contour on October 20, 2012

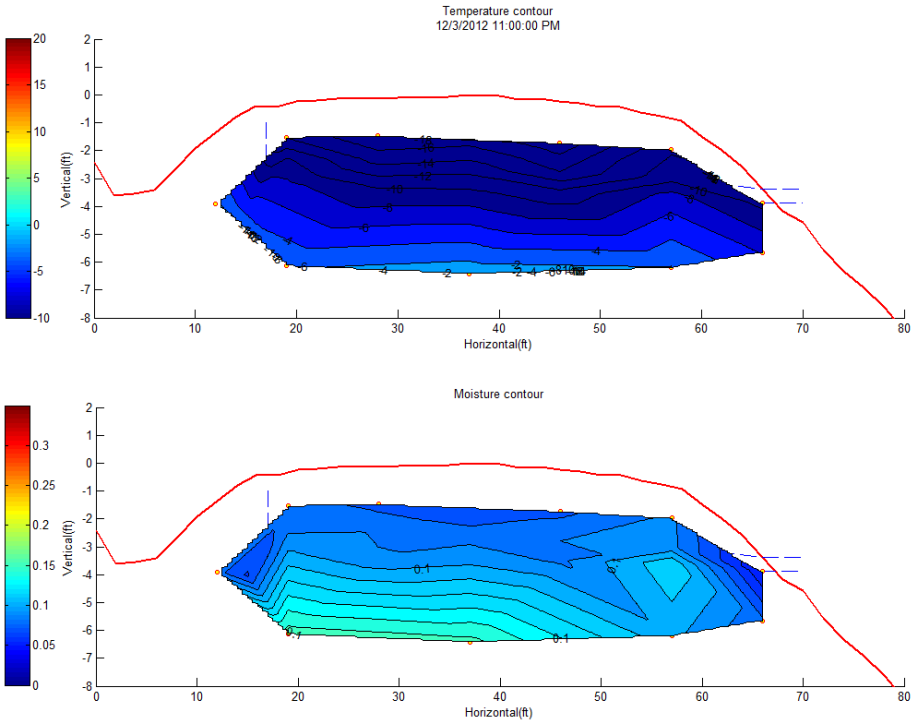

(c) Temperature and Moisture Contour on December 4, 2012

Figure 4.5 Temperature and Moisture Contour during Freezing Process

During Thawing Process

Figure 4.6 shows the temperature and moisture contours during the thawing process in 2013. The mean daily air temperature rose above 0°C on May 9, 2013, as shown in Figure 4.6(a). The temperature in the soil was still below 0°C and the unfrozen water content of the soil was still about 0.07 to 0.10. Figure 4.6(b) shows the temperature and moisture contours on May 25, 2013. The thawing front had penetrated to about 0.61 meters (2 feet) near the west edge of the road, and to 1.06 meters (3.48 feet) at the east edge. It was mentioned in a previous study (Zhang et al. 2014) that the frost boil phenomenon was observed during this time of the year. Similarly at sensor 22, located nearest to the drainage ditch, the unfrozen water content remained below 0.1, which indicated that the drainage ditch was still frozen at this time, and that there was no water supply from melting snow. All of the sensors showed that the moisture contents were below saturation. This demonstrates that no soft spots could be observed at this time of

the year. Figure 4.6(c) shows the temperature and moisture contours on June 26, 2013. The thawing front had protruded to 1.83 meters (6 feet) below the road surface, and a frozen core was evident in the center of the roadway. Again, since the moisture contents on west side of the road embankment showed large amounts of excess water during the previous freezing process, and because the west side is located adjacent to the drainage ditch, the moisture contents were expected to be higher than those on east side. Additionally, the frozen hard core in the center of the road embankment cut off the free water flow laterally and trapped the underground water at the east side of the roadway. Figure 4.6(d) shows the temperature and moisture contour on July 30, 2013. The thawing front had penetrated to 1.97 meters (6.4 feet) below the road surface, and the frozen core was thoroughly melted. The trapped saturation zone was released and was allowed to flow laterally out of the embankment. Meanwhile, the water stored in the drainage ditch and the ground water also provided additional water supply to the pavement structure; therefore, the saturation zone was expected to be even larger than before. Because of the presence of the wicking fabric, the east side of the embankment was relatively dry, demonstrating that the wicking fabric worked effectively to suck water out of the pavement structure.

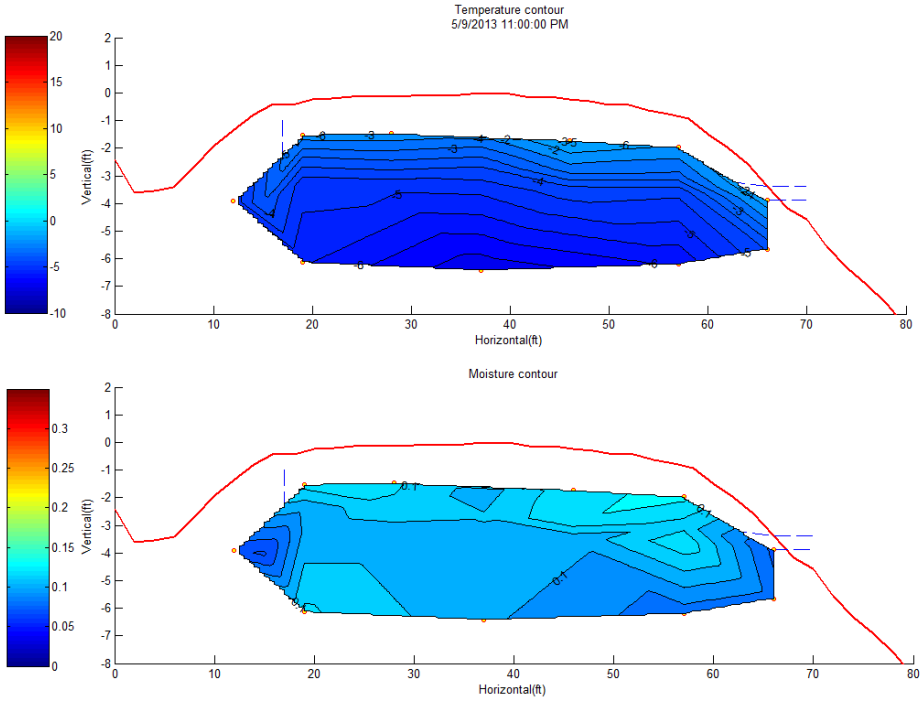

(a) Temperature and Moisture Contour on May 9, 2013

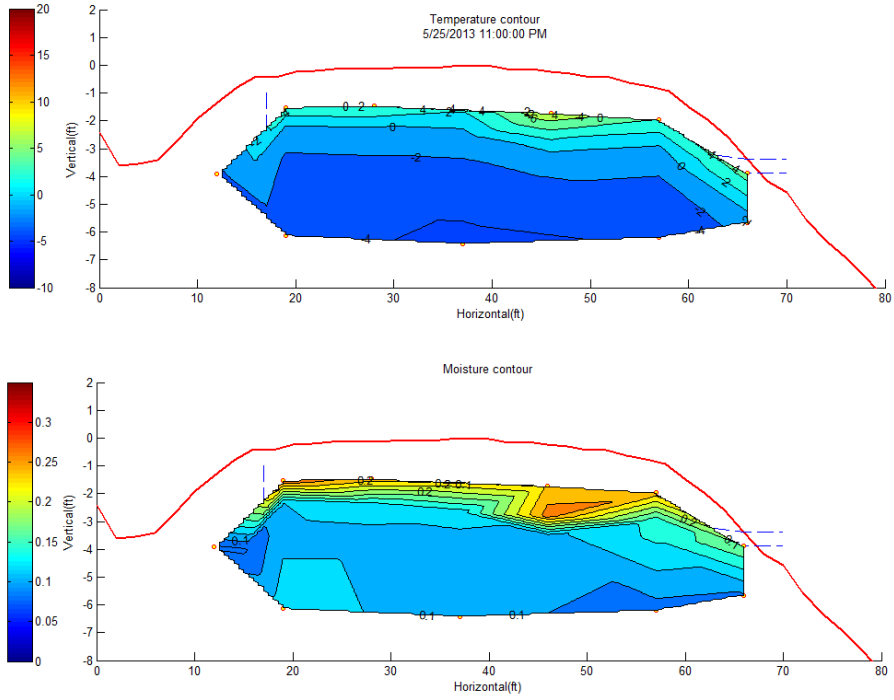

(b) Temperature and Moisture Contour on May 25, 2013

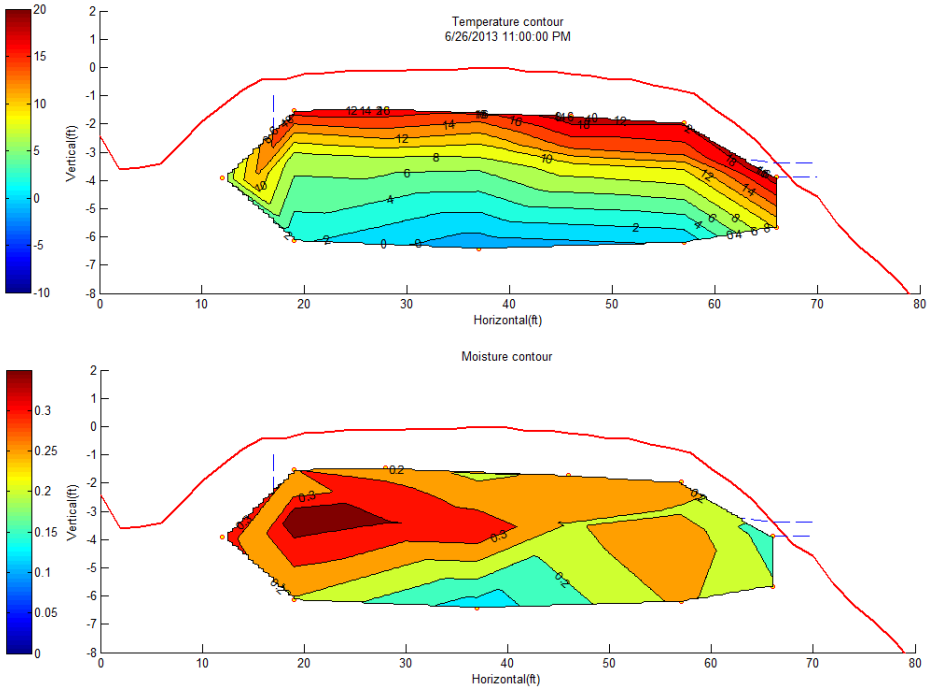

(c) Temperature and Moisture Contour on June 26, 2013

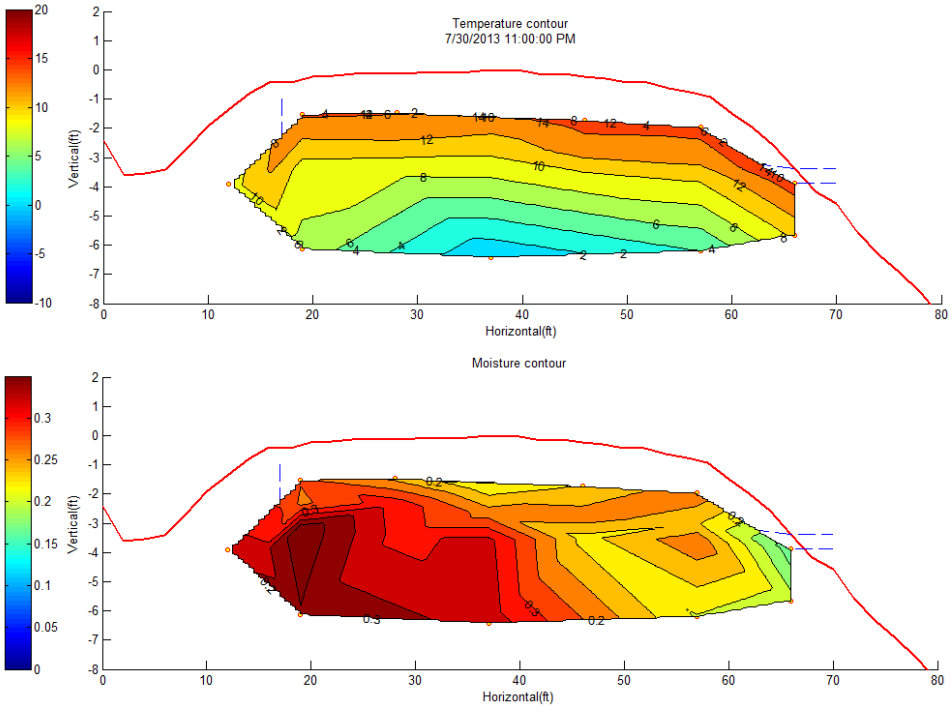

(d) Temperature and Moisture Contour on July 30, 2013

Figure 4.6 Temperature and Moisture Contours during Thawing Process

CHAPTER V WICKING FABRIC LONG–TERM PERFORMANCE

First of all, the moisture conditions at the beginning of freezing and thawing processes are critical to evaluate the effectiveness of the geotextile to mitigate frost heave and thaw weakening issues. Therefore, the moisture contours at the starting point of freezing and thawing processes are extracted and compared to demonstrate the improved pavement performance by implementing the geotextile. Secondly, there are several potential concerns need to be answered before the extensive application of the geotextile, such as the clogging effect, salt concentration effect, permanent deformation, mechanical failure and aging effect. In order to resolve those issues that might influence the long-term performance of the wicking fabric, field samples of the wicking fabric were collected from the Beaver Slide test site in July 2015. Then, a JOEL JXA-8530F Electron Microprobe was used to analyze the wicking fabric microstructures.

Moisture Condition Comparison during Freezing and Thawing Processes

During Freezing Process

It is critical to determine the moisture content distribution before the freezing front moves downward, because the severity of the thaw weakening in the following spring is directly related to the amount of water stored in the pavement structure before the freezing process started in the previous year. In other words, the soft spots in the following spring, if frost boiling was observed, would be expected where the saturation zones were observed before the freezing process started in the previous year. For purposes of this discussion, the moisture contours when the air temperature dropped below zero during the recorded four-year period were summarized and compared, as shown in Figure 5.1. It should be noted that the areas of the saturation zones decreased with time. For instance, there were two saturation zones that were connected together in 2010 and 2011 (Figure 5.1 (a) and (b)); however, the saturation zones became separated into two smaller zones on in 2012 (Figure 5.1(c)). The less the amount of water stored in the pavement structure, the less severity of the frost heave would be expected during the freezing process (less negative pore water pressure would be generated due to the water

phase changing from liquid state to solid state). Moreover, since the soil moisture contents were lower than the previous years, it took less energy to move the freezing front downward. In comparison, the freezing front had already penetrated to 0.9 meters (2.95 feet) on October 11, 2012, which was about 0.3 meters (0.98 feet) deeper than the previous year. Furthermore, the saturation zone continued to decrease at the bottom of the roadway in year 2013, as shown in Figure 5.1(d). This phenomenon could be apparent because: (1) precipitation variation may cause such variations in the soil moisture content distribution, (2) the wicking fabric worked effectively to reduce the moisture content in the soil. Because the rainfall event summary presented in Table 4.1 indicated that there were no significant rainfall events that occurred right before the selected days, precipitation was not the reason that caused the decrease in soil moisture contents. Therefore, the wicking fabric did reduce the water content on east side of the roadway embankment, and reduced the size of saturation zone on west side of the road. However, the performance of the wicking fabric to drain the water out needed to be further evaluated during the spring thawing process to validate its efficiency.

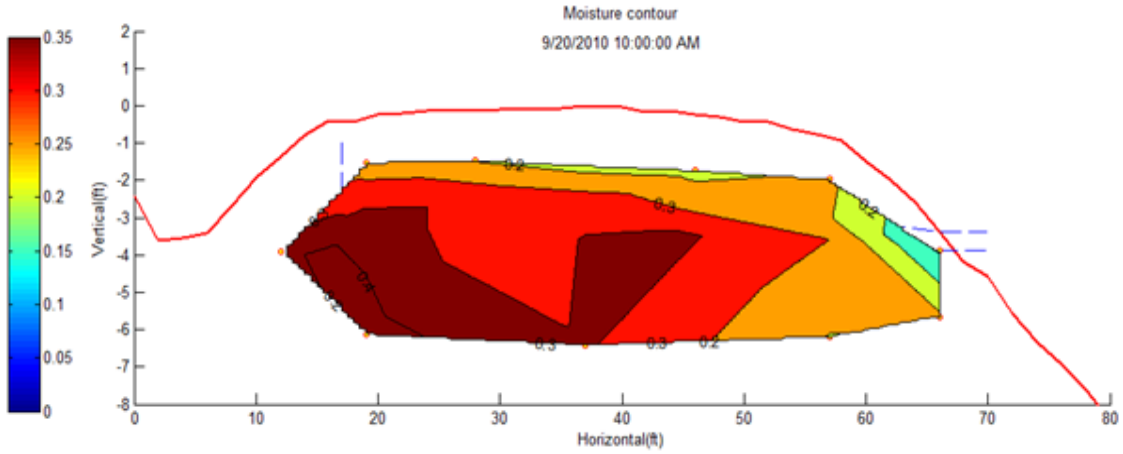

(a) Moisture Contour on September 20, 2010

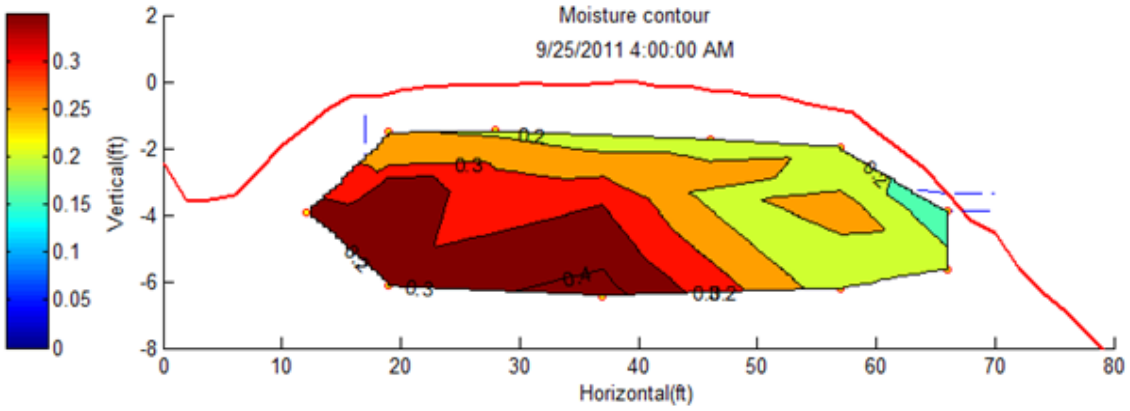

(b) Moisture Contour on September 25, 2011

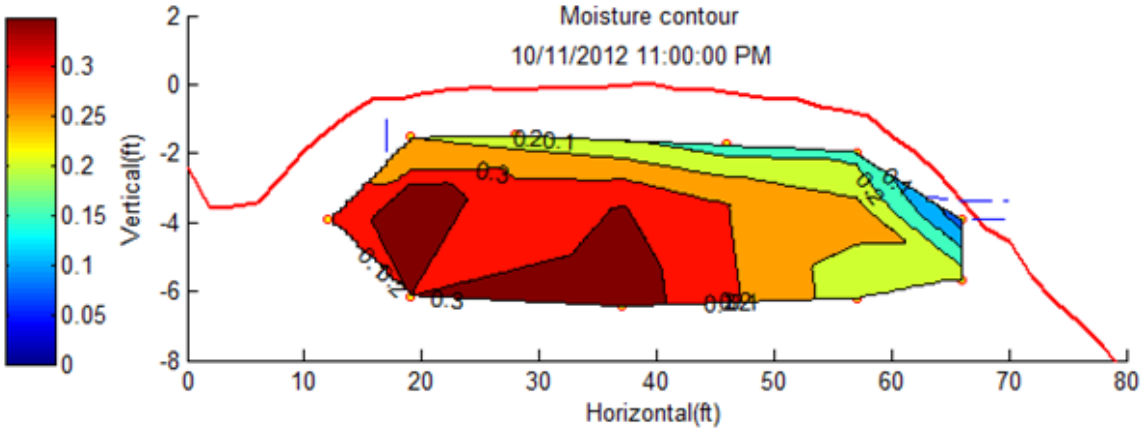

(c) Moisture Contour on October 11, 2012

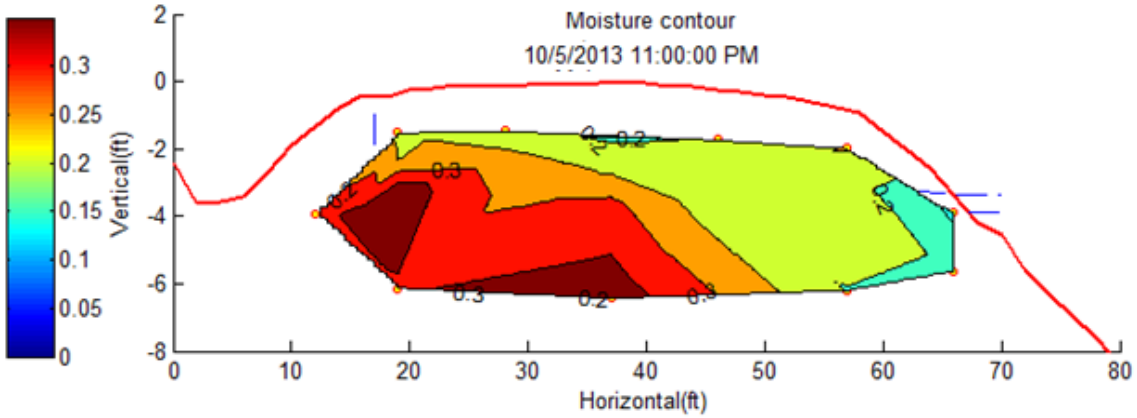

(d) Moisture Contour on October 5, 2013

Figure 5.1 Moisture Contours before Freezing

During Thawing Process

It was mentioned in a previous study (Zhang et al. 2014) that the frost boil phenomenon was observed in late April or early May and the worst scenario was expected in late May, it is critical to evaluate and compare the soil moisture contours at this time for the monitored four years.

Figure 5.2 shows the moisture contours in late May of each year. Firstly, the unfrozen water contents for sensor 22, which located nearest to the drainage ditch, remained below 0.1 within the monitored four years. This phenomenon indicated that the drainage ditch was still frozen at this time, and that there was no water supply from melting snow. Therefore, the water source that caused thaw weakening issue was major resulted from the melting of frozen soil within the pavement structure.

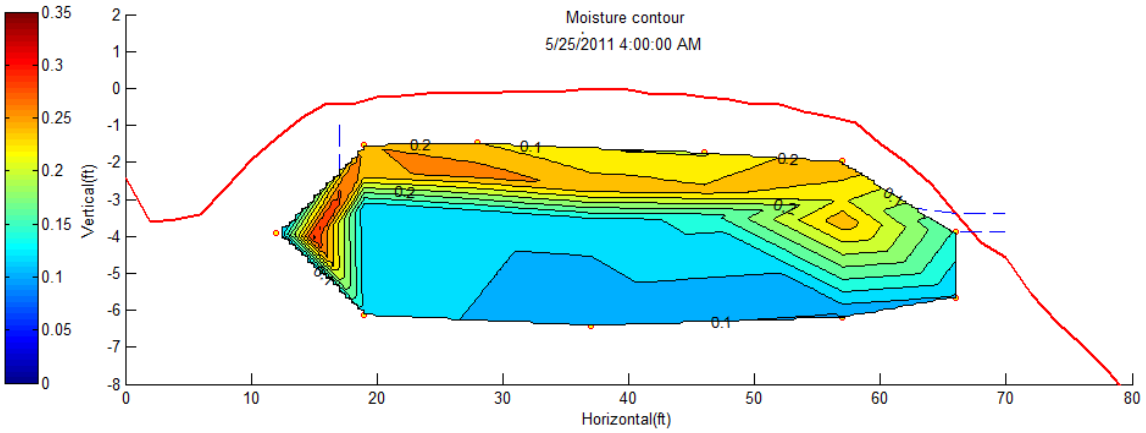

(a) Moisture Contour on May 25, 2011

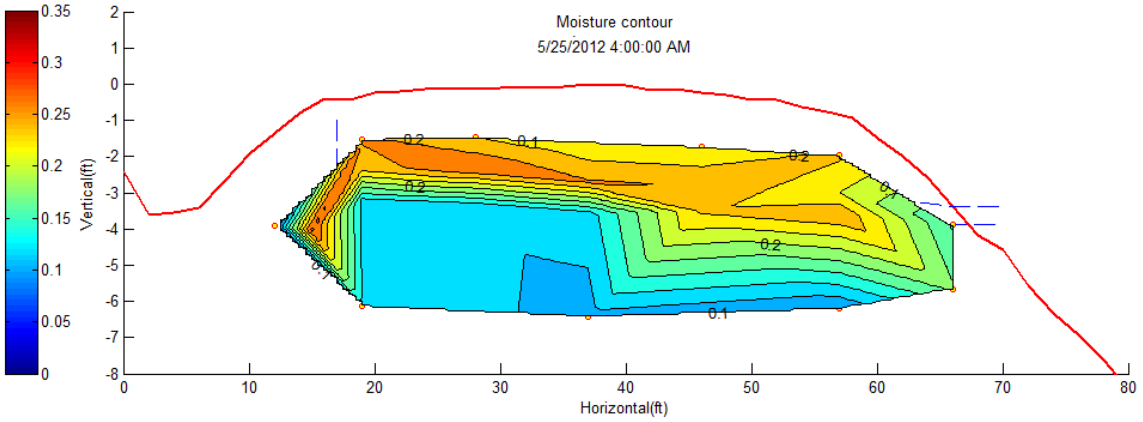

(b) Moisture Contour on May 25, 2012

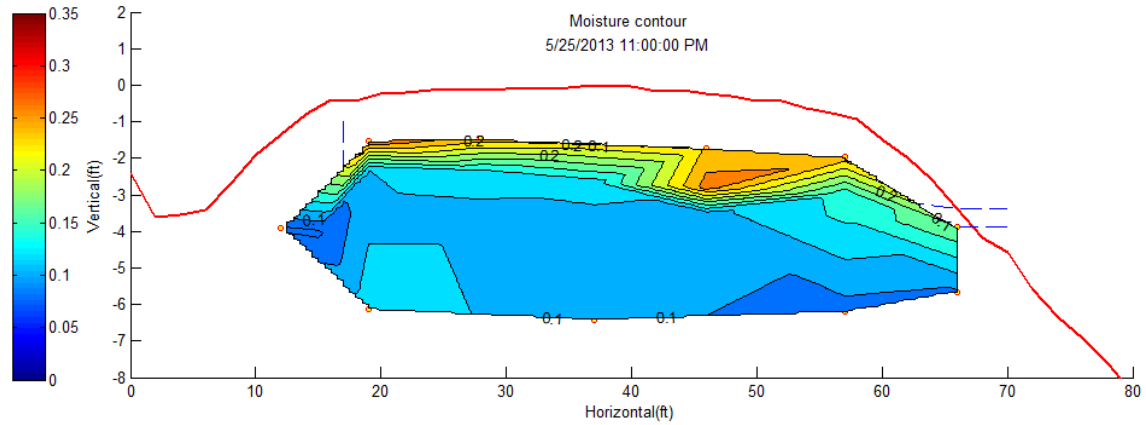

(c) Moisture Contour on May 25, 2013

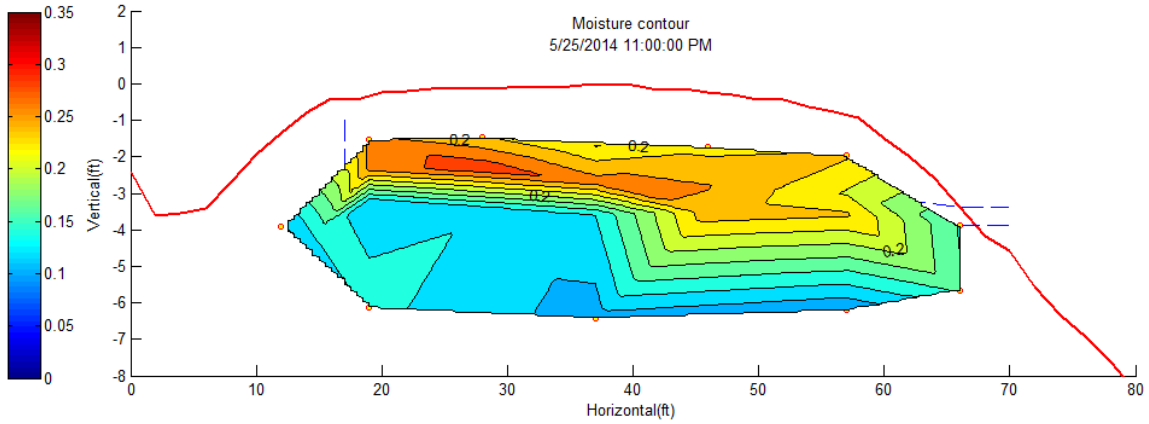

(d) Moisture Contour on May 25, 2014

Figure 5.2 Moisture Contours during Thawing Process

Secondly, it is important to point out that the mean monthly temperature for May, 2013 was lower than in previous years, so the thawing front only penetrated to 1.22 meters (4 feet) on the east side and 0.76 meters (2.5 feet) on the west side. For the other years monitored, the distance between the thawing front and the 0 °C isothermal curve increased each year. This phenomenon can be explained by referring to the moisture contour during freezing process, as discussed in the previous section. Since the saturation zone in the pavement structure was decreasing during the monitored four years, the total amount of water stored in the pavement structure (including capillary water extracted from shallow groundwater) was also decreasing. Since the specific water capacity was

larger than soil, the distance between thawing front and the 0 °C isothermal curve was expected increasing with time.

Thirdly, the highest moisture content areas were all located on the west side of the embankment, but no saturation zone was observed during the thawing process in the monitored four years. This phenomenon proved that the wicking fabric successfully eliminated the frost boiling issues. Moreover, the thawing front on east side of the embankment was deeper than that on west side and reached to the elevations where the two layers of wicking fabrics were buried. This phenomenon indicated that the wicking fabric on east side of the pavement structure was partially functional and started to laterally drain the water out of the pavement structure in late May, 2014, as shown in Figure 5.2(d).

SEM Analyses

In addition to the macroscopic study discussed above, the interaction between the wicking fabric and the surrounding soils on a microscopic level was investigated. As mentioned previously, there were several concerns about the long-term performance of the wicking fabric, specifically the clogging effect, salt concentration effect, permanent deformation, mechanical failure and aging effect. In total, 30 samples were analyzed; the detailed process and illustration regarding SEM analyses follows.

Clogging Effect

Figure 5.3(a) presents the woven structure of a sample at Beaver Slide with ×55 magnification. Large amounts of soil particles were detained on the surface of the wicking fabric. Because the soil contained approximately 6% of fines, the fine materials blocked the deep grooved drainage paths. Figure 5.3(b) shows a closer view of the wicking fabric at the surface with ×350 magnification. It further illustrates the fact that the deep grooved drainage paths were completely filled with fine soil particles. In comparison, Figure 5.3(c) shows the wicking fabric fibers just beneath the surface layer. The deep grooves beneath the surface were much cleaner than those above, and there were very few particles that had been detained in the drainage paths. In other words, the

fibers of the wicking fabric at surface served as a protective layer, preventing the fine soil particles from penetrating deeper into the fabric structure. Figure 5.3(d) shows the comparison of the wicking fibers on the surface and the fibers just beneath the surface. It can be visualized from the figures that even though the wicking fabric fibers on surface were filled with fine soil particles, the wicking fibers beneath the surface still work effectively to laterally drain water out of the pavement structure. It is worth noting that it is not fair to evaluate if the wicking fabric is clogged based upon the fibers on the surface since "surface" is a theoretic term and difficult to define during the SEM analyses. If too many soils are left on the surface of the wicking fabric, there is no doubt that the wicking fabric will be covered by the soils. On the other hand, if we take all the surface soil away, the evaluation for the clogging effect is not objective. It seems more reasonable to evaluate the clogging effect based upon the wicking fibers below the surface. From Figures 5.3(c) and 5.3(d), it is concluded that clogging is not a concern for the wicking fabric.

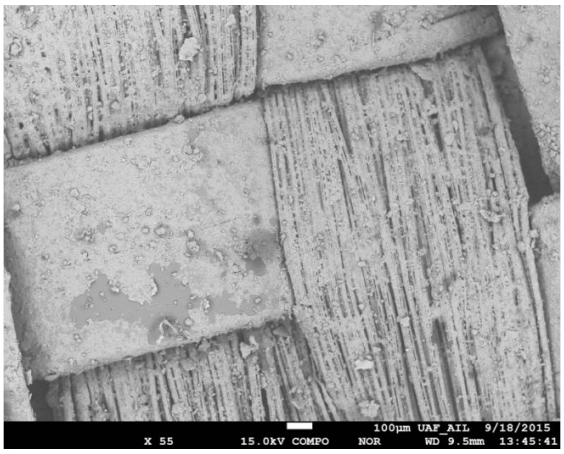

(a) Intact Sample (Sample 4)

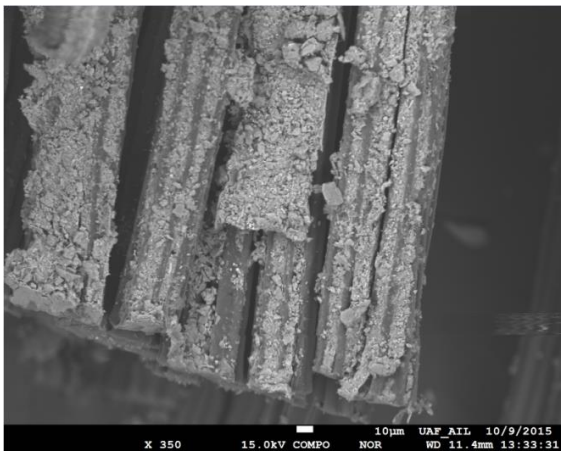

(b) Surface Clogging (Sample 20)

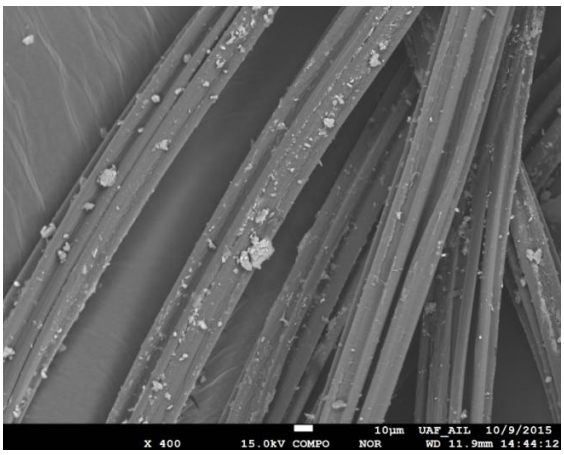

(c) Beneath Surface (Sample 25)

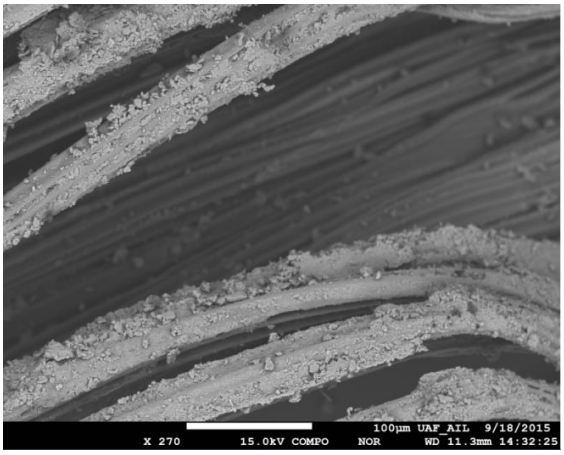

(d) Wicking Fabrics Comparison

Figure 5.3 SEM Images of Clogging Effect

Permanent Deformation and Mechanical Failure

Figure 5.4 presents the SEM images of samples that suffered permanent deformation and mechanical failure. Figure 5.4(a) presents images of new wicking fabric, which was brand new. It was apparent that the wicking fabric fibers under the woven polypropylene yarns had already experienced some permanent deformation, and that the deformation was in the vertical direction. The pressure applied in manufacturing process may have caused this deformation, or it may have occurred during the transportation process. Figure 5.4(b) shows SEM images of the wicking fabric that was collected from the field. The permanent deformation observed in the new materials had further increased. Due to additional vertical pressure, the wicking fabric fibers were nearly flattened, and the deep grooves were not able to hold water under unsaturated conditions. Furthermore, Figure 5.4(c) presents the front view of the wicking fabric; deep grooves are seen not only in the vertical direction, but deep grooves also tended to close in the horizontal direction.

Another mechanical failure known as “puncturation” is illustrated in Figure 5.4(d). “Puncturation” refers to the puncturing of the soil fibers by the large soil particles that were detained on the wicking fabric surface. The large soil particles, especially those with sharp edges, acted as a cutting edge that severred the deep grooves of the wicking fabric. This likely occurred due to the high overburden soil pressures and the dynamic traffic

loads applied to the road surface. The drainage paths were broken and became unable to continue to laterally transport water; however, this phenomenon was only observed in 5 of the 30 samples collected from the field. According to the observed macroscopic results at the Beaver Slide, it seems that neither permant deformation nor puncturation were major concerns, possibly for two reasons (1) there were relatively less percentage of the wicking fabric having permant deformation or puncturation, and (2), surrounding fine soil particles might have "bridging effect" for water transport at locations where permant deformation or puncturation occurred.

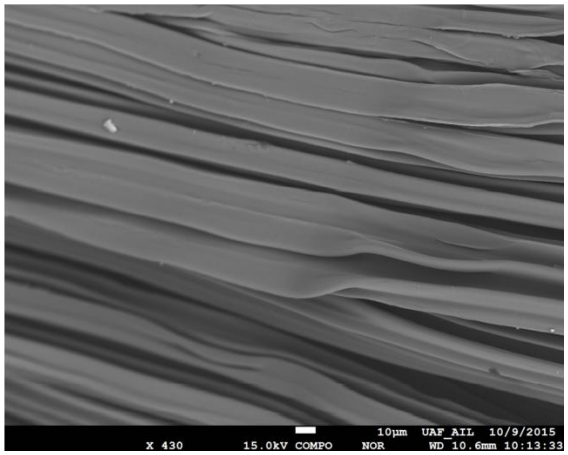

(a) New Wicking Fabric (Intact Sample 4)

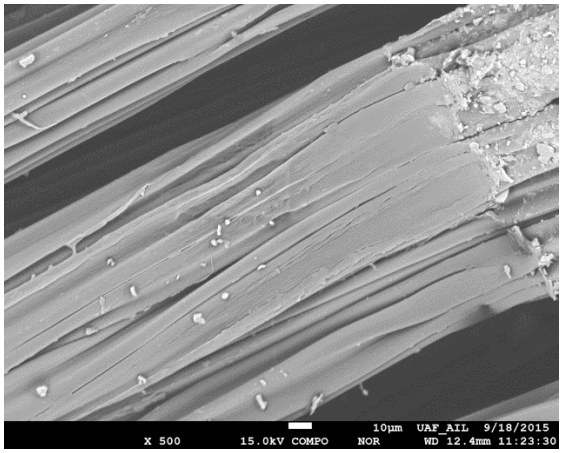

(b) Permanent Deformation (Sample 1)

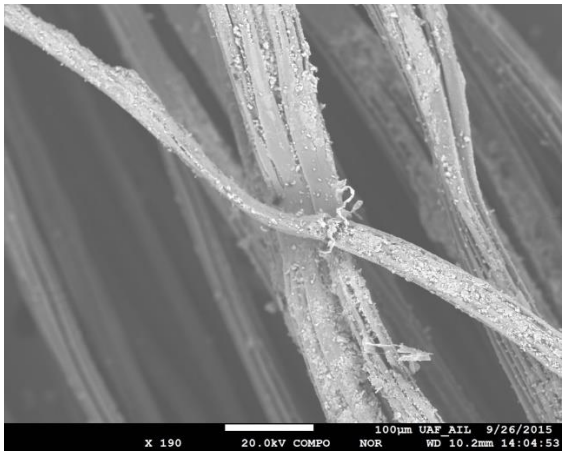

(c) Permanent Deformation (Sample 16)

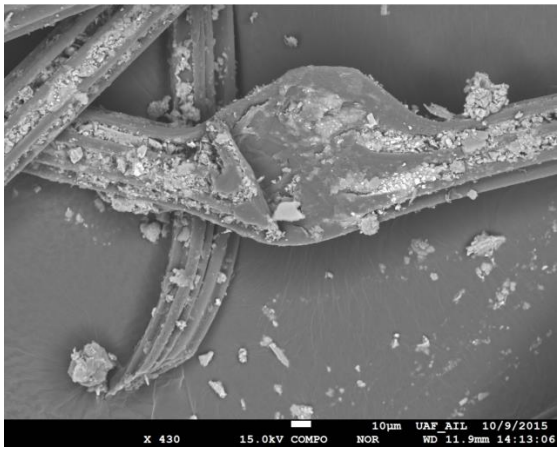

(d) Beaver Slide Sample 17

Figure 5.4 SEM Images of Mechanical Failure

Aging

Because the wicking fabric is buried under the soil, another concern involves the wicking fabric's physical and mechanical aging issue, as shown in Figure 5.5. Figure 5.5(a) shows the aging severity of the wicking fabric fibers under the woven polypropylene yarns. Because the wicking fibers on the surface were directly in contact with the soil particles, the aging phenomena were usually observed in the fibers located at the surface of the fabric. Figure 5.5(b) shows the wicking fabric fibers at the surface without the woven polypropylene yarns. As believed, the aging phenomenon was likely due to direct contact with the soil particles. The aging effect at the bottom of the deep grooves was more severe than in the other areas of the wicking fabric. In comparison, Figure 5.5 (c) and (d) show the wicking fabric beneath the surface. No obvious aging effect was observed below the surface layer, and the deep grooves were much cleaner than those of the fibers on surface.

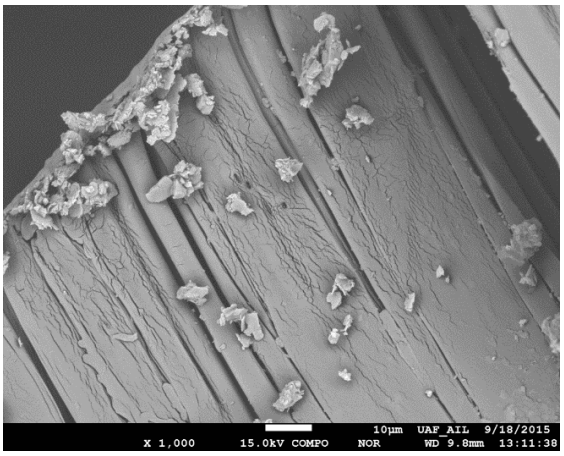

(a) Beaver Slide Sample 3

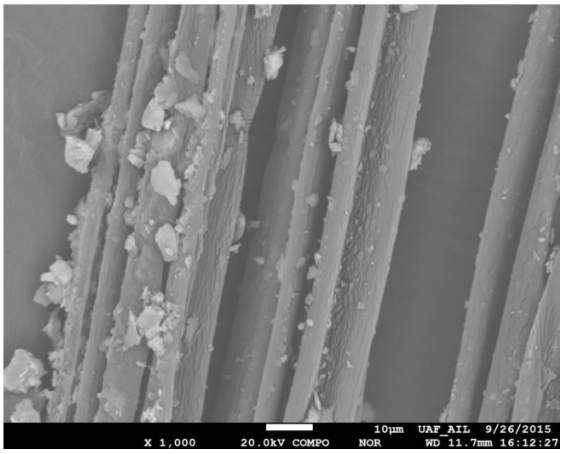

(b) Beaver Slide Sample 11

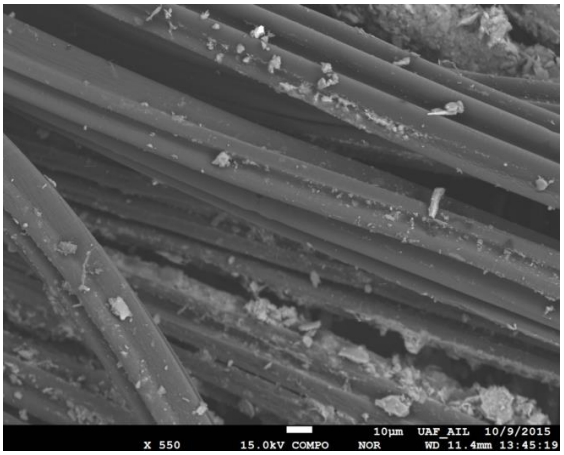

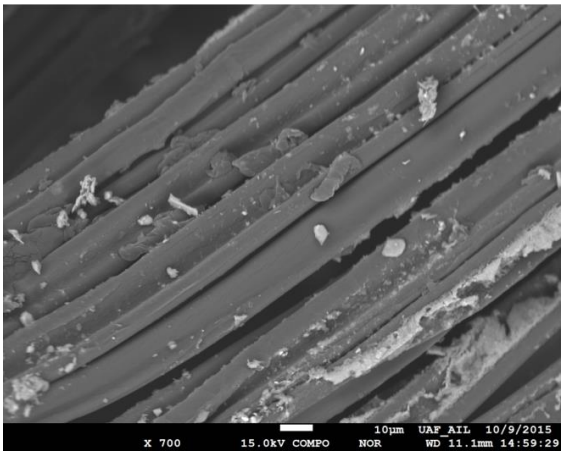

(c) Beaver Slide Sample 21 (d) Beaver Slide Sample 26

Figure 5.5 Aging Effect

Table 5.1 summarizes the SEM analyses results. In general, all wicking fabric fibers on the surface suffered from the clogging effect. Clogging at the surface of the wicking fabric and permanent deformation were observed in every scanned sample. However, only 6.67% of the wicking fabric fibers beneath the surface suffered from the clogging effect. This indicates that even though the surface was contaminated and the drainage paths were blocked, the wicking fibers beneath the surface were well protected and worked effectively as a drainage material to transport water laterally under unsaturated conditions. Additionally, the permanent deformation was observed in every sample under the polypropylene woven area. The permanent deformations resulted from one, or both of the following two processes: (1) high pressure during the manufacturing process, and (2) high vertical overburden soil pressure and dynamic traffic load during its service life. The permanent deformation would likely affect the wicking fabric's long-term performance, since the drainage paths were either cutoff or narrowed down, and the deformation would continue to develop with time. The aging effect and mechanical failure were not considered to be major concerns that would influence the long-term performance of the wicking fabric. Therefore, permanent deformation is the major potential issue that needs to be taken into consideration in evaluating the wicking fabric long-term performance.

Table 5.1 SEM Analyses Summary

<table>
<tr><th rowspan="2">Sample</th><th rowspan="2">Total</th><th rowspan="2">Observation</th><th colspan="2">Clogging</th><th rowspan="2">Mechanical Failure</th></tr>
<tr><th>Surface</th><th>Beneath</th></tr>
<tr><td rowspan="5">Beaver Slide</td><td rowspan="5">30</td><td>Count</td><td>30</td><td>2</td><td>5</td></tr>
<tr><td>(%)</td><td>100</td><td>6.67</td><td>16.67</td></tr>
<tr><td>Observation</td><td colspan="2">Permanent Deformation</td><td>Aging</td></tr>
<tr><td>Count</td><td colspan="2">30</td><td>7</td></tr>
<tr><td>(%)</td><td colspan="2">100</td><td>23.33</td></tr>
</table>

Salt Concentration Effect

Another potential issue is that the salt in soil and water may detain in the wicking fabric and block the drainage yarns. In order to evaluate the severity of salt concentration,

NaCl solutes were made with different concentrations, including 10 g/L, 20 g/L, 30 g/L, 40 g/L and 50 g/L. Two types of samples were prepared, namely air-dried samples and rewetted samples. The air-dried samples are prepared by air-dried the wicking fabric that be dipped into the aimed salt solution. The rewetted samples were prepared by washing the air-dried samples with water and then air-drying them. Figure 5.6 demonstrates the spectral scanning results. The scanning area shows part of the wicking fabric that was scanned and analyzed. The full-scale spectrum analysis gives the raw scanning data, which indicates the total number counts for each chemical element preselected in the periodic table. Based on the selected chemical elements from the periodic table, the spectral imaging shows the concentration of the scanning area. Since the wicking fabric is made of polypropylene yarns, the carbon element was identified as the representation of the wicking fabric. Meanwhile, the soluble salt used in the salt concentration test is sodium chloride (NaCl), both Na^+ and Cl^- ions are considered as the representation of the severity of concentration. In general, the brighter shown in the carbon element spectral imaging, the less salt concentration it represents. In contrast, the brighter shown in the sodium and chloride elements, the more salt concentration shall be expected.

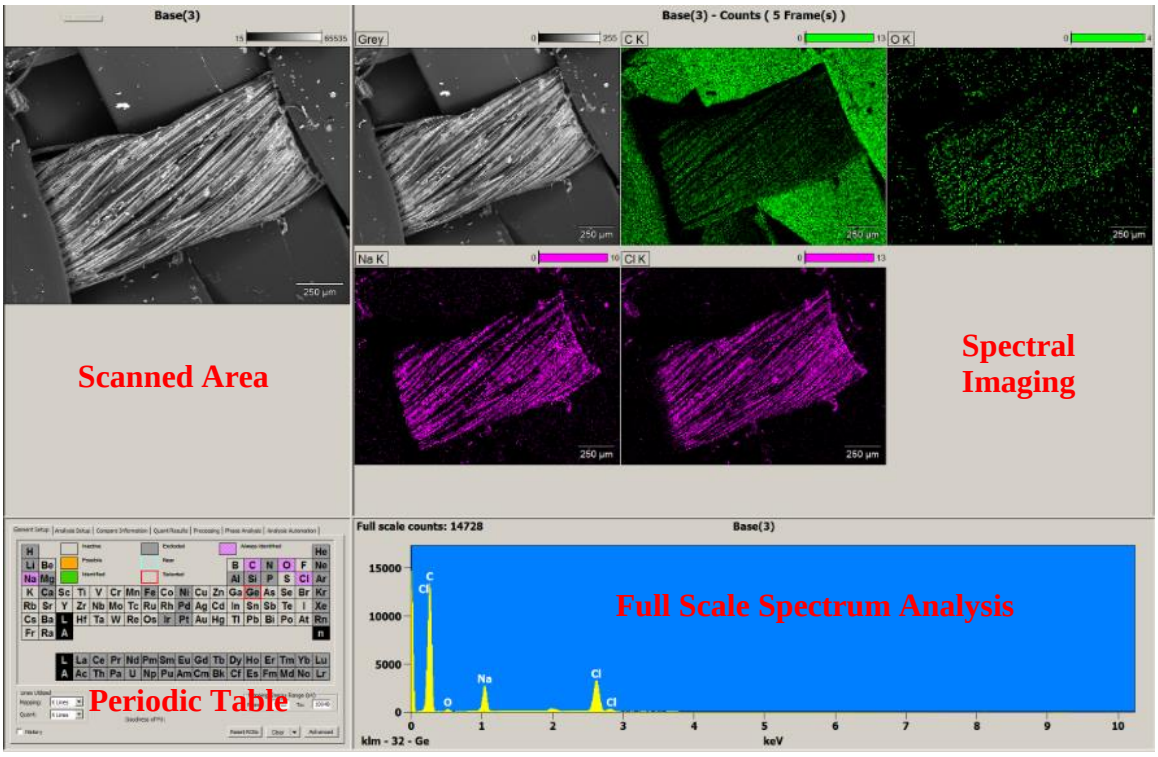

Figure 5.6 Salt Concentration Test Result Demonstration

Figure 5.7 shows the salt concentration test results for both air dried and rewetted samples. Since wicking fabric yarns represents better the severity of salt concentration, the selected scanning area only included the hygroscopic nylon yarns rather than the polypropylene yarns. It is reasonable to expect that the salt detained on the deep grooves of the wicking fabric will increase with the increment of salt concentration in solute. The bar at top of each figure shows the severity level of salt concentration. The test results showed that the average concentration levels for drying samples were 10, 13.5, 13.5, 15.5 and 22 for salt solute with concentrations of 10 g/L, 20 g/L, 30 g/L, 40 g/L and 50 g/L, respectively. The bright strip shape of sodium and chloride spectrum images indicated that concentration areas mostly occurred in the deep grooves of the nylon yarns. For comparison, the severity of salt concentration for rewetting samples were approximately within the same magnitude, only slightly increased from 2.5 to 9.5 when salt concentration of solute increased from 10 g/L to 50 g/L. Since the salt used in the test was sodium chloride, which is a common type of soluble salt, it is reasonable to expect that most of the salt concentrated on the wicking fabrics would be washed away during the rewetting process. Table 5.2 summarizes the test results for salt concentrationt test results. In sum, even though salt concentrated in the deep grooves in the wicking fabric yarns during the drying process, the salt would be washed away due to the solubility of the salt used in the test.

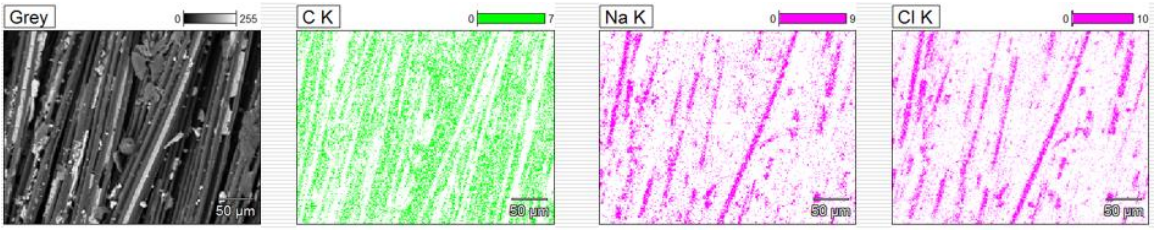

(a) Drying Sample, 10 g/L

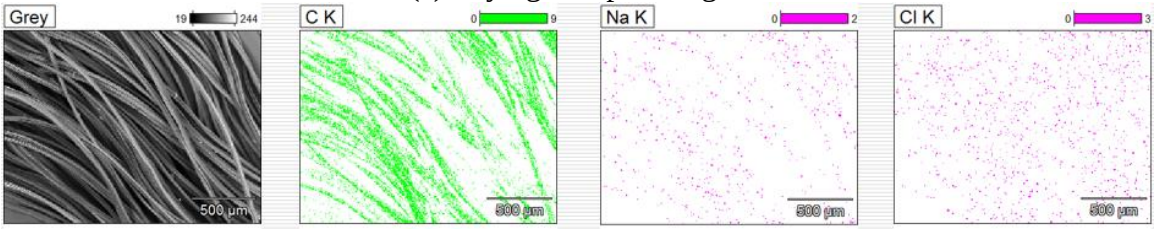

(b) Rewettomg Sample, 10 g/L

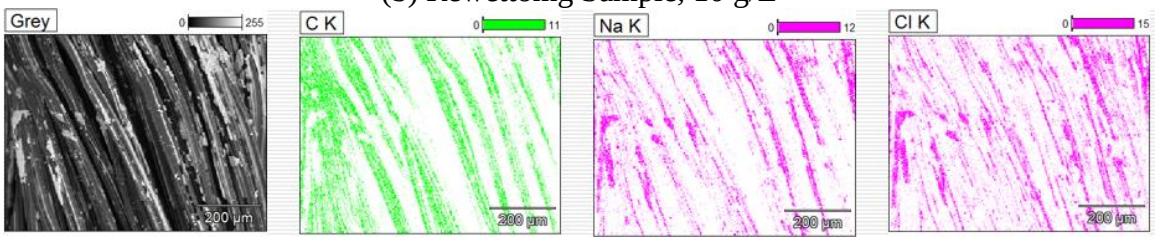

(c) Drying Sample, 20 g/L

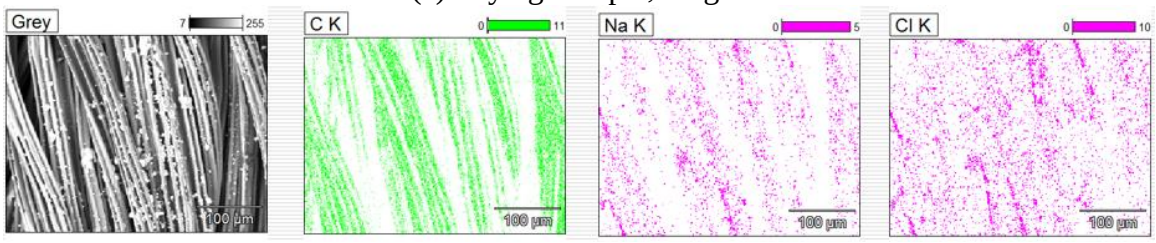

(d) Rewetting Sample, 20 g/L

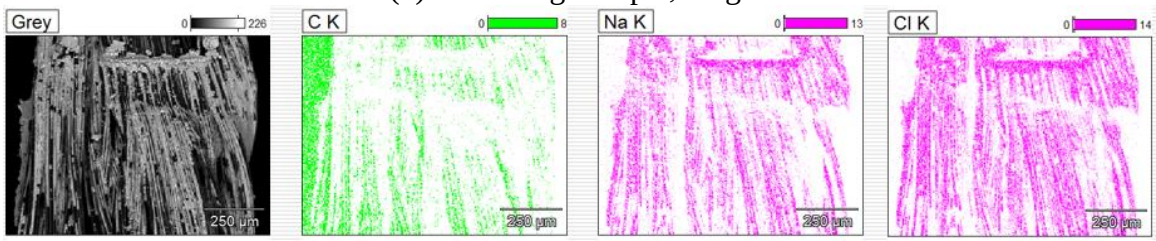

(e) Drying Sample, 30 g/L

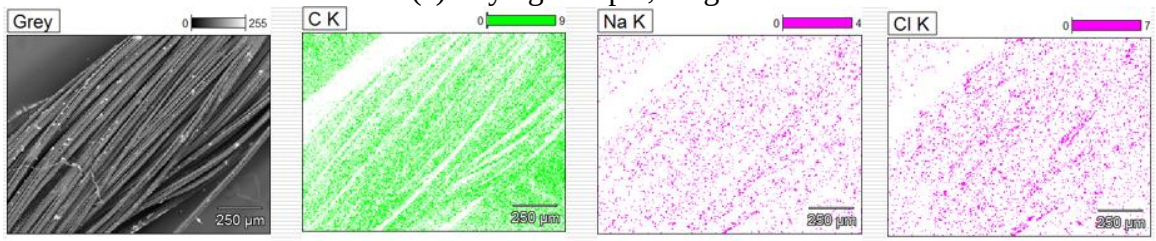

(f) Rewetting Sample, 30 g/L

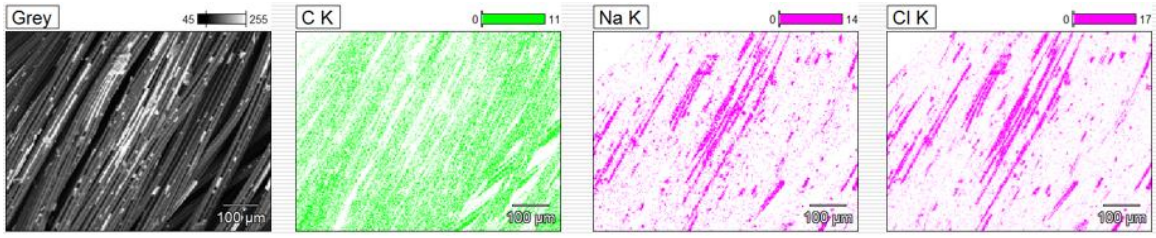

(g) Drying Sample, 40 g/L

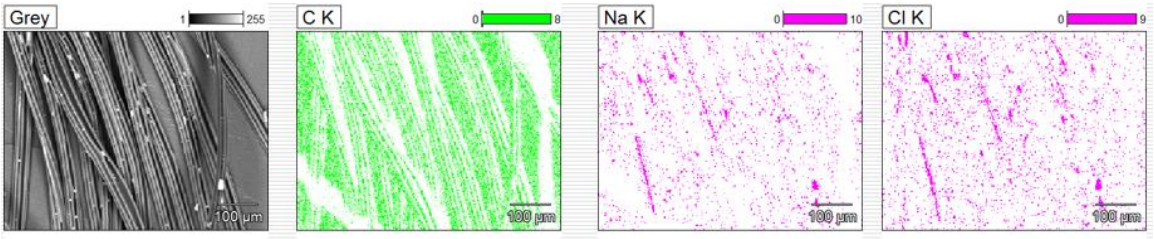

(h) Rewetting Sample, 40 g/L

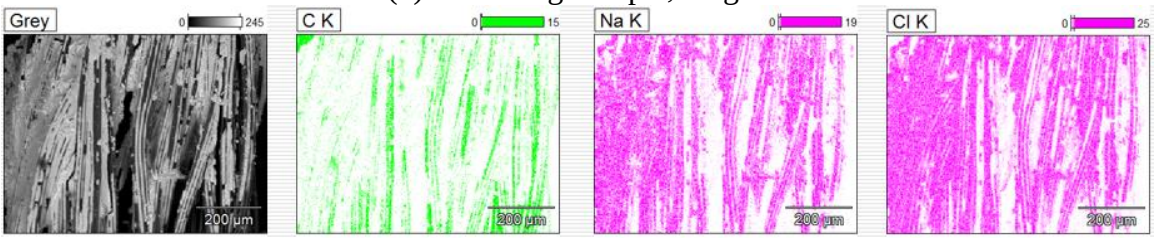

(i) Drying Sample, 50 g/L

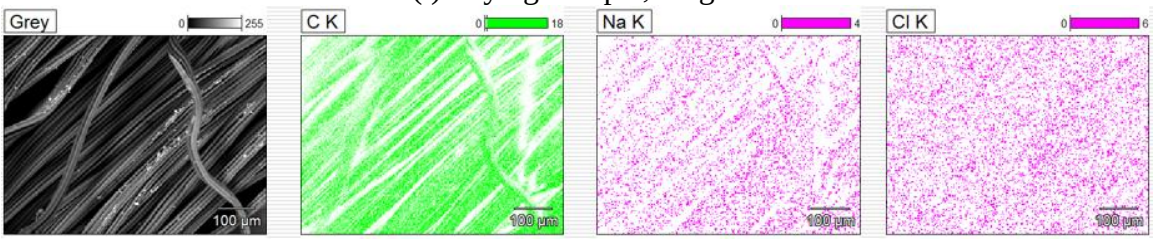

(j) Rewetting Sample, 50 g/L

Figure 5.7 Salt Concentration Test Results

Table 5.2 Salt Concentration Test Result Summary

Salinity (g/L, or ppt)	Type	Chemical Components	
		Na^+	Cl^-
10	drying	9	10
	rewetting	2	3
20	drying	12	15
	rewetting	5	10
30	drying	13	14
	rewetting	4	7
40	drying	14	17
	rewetting	10	9

50	drying	19	25
	rewetting	4	6

DISCUSSIONS

Factors Influencing the Occurrence of Frost Boils/Soft Spots

As previously mentioned (Zhang et al., 2014), the frost boils often occurred during the end of April through May each year. Based on the comparisons of the pavement performance during the monitored four years, the water sources that are available to form the frost boils came from the thawing of *in situ* ice lenses that developed in the pavement structure due to frost heave in the previous winter. The moisture content of the pavement structure at the beginning of the freezing process was one of the major factors that determined the intensity of the frost heave and the subsequent thawing in the next year. The larger the fully saturated zones were in the pavement structure, the more suction or negative pore water pressure (due to water expansion during the freezing process) it would generate. Since the freezing process penetrated the pavement structure from the top to the bottom, the only water source must be from the shallow water table beneath the pavement structure. Higher suction values would further increase the moisture content in the pavement structure and cause a zone of over saturation. The melting water from the over-saturated zone would provide sufficient water during the following spring to create soft spots at the surface, because the water was forced to the road surface when the soil beneath was still frozen.

Another factor influencing the severity of the frost boils is when the thawing front penetrated down to the bottom of the pavement structure. The thawing front penetrated to the bottom of the pavement structure in late July or early August, which was almost three months after the thawing season began. Because the frozen soil in the west side of the roadway held a large amount of frozen water, it took a larger amount of solar energy to

melt the frozen soil. The only drainage path for the melting snow and runoff water was to flow through the pavement structure. This would further reduce the soil stiffness and intensify the frost boil issue. Furthermore, the center of the pavement structure formed a hard, frozen core during the melting season. The frozen core altered the water flow direction and trapped a large amount of water in the west side of the pavement structure. As discussed previously, the larger the saturation zone that existed in the pavement structure, the more severe the frost boil issue would be the following spring.

It is also worth noting that a large amount of rainfall would cause another issue called pressurized water overflow, which may also have generated soft spots on the road surface in summer time. Rainfall duration served as a more deteriorating factor to the pavement performance than rainfall intensity. The soft areas would heal up if there were periods of no rain. The moisture contents in the pavement structure beneath 0.47 meters (1.5 feet) experienced short periods of time overly saturated. By carefully examining the rainfall events summary, it is seen that there were several days of rainfall before the sudden increases in moisture content. Since the road prism was built on a side hill, the water naturally flows from west to east. Also, Beaver Slide is approximately 11° downhill heading north, which made the hydraulic gradient the highest at the test section. These factors are evidence that the sudden increases in moisture content were due to pressurized water overflow to the road surface. Although the two issues presented the same superficial phenomena, the mechanisms causing the phenomena were different. For the obtained data in the past five years, it seems that the wicking fabric has mitigated the frost boils caused by both mechanisms.

Wicking Fabric Long-Term Performance

Data collected during four years of monitoring indicates that the wicking fabric has worked effectively to prevent the frost heave and thaw weakening issues previously observed at Beaver Slide. During the rainfall events, the water could be drained out 1-2 days after the rainfall stopped. Moreover, the moisture contents were gradually decreasing within the pavement structure before the freezing process. This indicates that the water supply for frost heave was decreasing, and that the moisture contents during the next

thawing process were also decreasing. As shown in Figure 5.2, there was no saturation zone present in the pavement structure during the thawing process. Additionally, the wicking fabric successfully drained water laterally out of the pavement structure within several hours, even after heavy rainfall events. The moisture contents near the wicking fabric were much higher than moisture contents in other areas, demonstrating that the fabric worked effectively to transport the water out of the embankment. The moisture contents in east (dry) side of the pavement structure reached equilibrium generally within 1 day of significant rainfall events.

In addition to macroscopic field observations of the improved road performance, the microscopic SEM analyses also partially answered the questions proposed at the start of this report. One of the major concerns was whether the fines in the soil would be retained in the deep grooves and potentially restricted the drainage path. Figure 5.3 clearly shows that even though the wicking fabric fibers at surface experienced the clogging effect, the fibers beneath them were relatively clean and well protected by the surface fibers. A new issue was that the permanent deformation due to high vertical pressure may narrow down or even cutoff the deep grooves, blocking their ability to laterally transport water in unsaturated conditions. This deformation may be induced by the high pressure during manufacturing process or traffic load. More research is needed in this direction. Aging and mechanical failure was observed in the SEM analyses; however, the occurrence percentage was relatively low and was not a major concern for the long-term performance of the wicking fabric.

CHAPTER VI CONCLUSIONS

The Beaver Slide project has been monitored for more than five years, and the results indicate that the wicking fabric has successfully eliminated the “frost boils” at the site. The conclusions are listed as follows:

1. The soft spots observed during the early spring were caused by the ice formation and thaw weakening of the soils; however, the soft spots observed after heavy rainfall resulted from pressurized water flow. Although the phenomena were similar, the mechanisms were entirely different.
2. The severity of the thaw weakening in spring is relative to the moisture content present in the pavement structure before freezing begins at the start of the previous winter. The monitoring data shows that the moisture contents were decreasing, and that the saturated zones were smaller each year after the fabric was installed. Moreover, the moisture contents in the pavement structure were not observed to exceed the saturation moisture contents. This indicates that the wicking fabric worked successfully to eliminate the ice formation and subsequent thaw weakening issue during the past five years. The wicking fabric exhibits promising long-term performance results; however, additional monitoring and data analysis should be performed to establish long-term performance.
3. Clogging was only observed in the surface fibers of the wicking fabric. The wicking fabric fibers beneath the surface layer were relatively clean. The clogging effect was not considered to be a major issue for the application of the wicking fabric.
4. The permanent deformation might be an issue that will affect the long-term performance of the wicking fabric. The deformed, deep grooves or drainage paths will reduce the amount of water that the wicking fabric can laterally transport. The permanent deformation may develop further over time due to high vertical pressure induced by the dynamic traffic loads and the overburden soils. The wicking fabric implementation depth and its influence on long-term performance should be studied further.

5. Mechanical failure and aging of surface fibers were observed in a limited number of samples. Mechanical failure may be caused by compaction during the construction process and high vertical pressure during its service life. Aging was observed in the surface fibers of the wicking fabric, where fibers were directly in contact with the surrounding soils.
6. Salt concentration was observed for drying samples, but can be washed away by water due to the solubility of the sodium chloride used in the test. For further studies, insoluble salt (such as Calcium Carbonate $CaCO_3$) shall be used to evaluate the effect of salt concentration on the wicking fabric long-term performance.

REFERENCES

Chamerlain, E. J. (1987). "A Freeze-Thaw Test to Determine the Frost Susceptibility of Soils." U.S. Army Corps of Engineers, Cold Regions Research and Engineering Laboratory (CRREL), Special Report 87-1.

Casagrande, A. (1947). "Classification and Identification of Soils." Proceedings, American Society of Civil Engineers, Vol. 73(6), pp. 283.

Csathy, T. I. and Townsend, D. L. (1962). "Pore Size and Field Frost Performance of Soils" Highway Research Board Bulletin, No.331, pp. 67-80.

Taber, S. (1930b). "Freezing and Thawing of Soils as Factors in the Destruction of Road Pavements." Public Roads, Vol. 11(6), pp. 113-132.

Takagi, S. (1978). "Segregation Freezing as the Cause of Suction Force in Ice Lens Formation." Cold Regions Research and Engineering Laboratory (CRREL), Report No. 78-6, pp, 12.

Takagi, S. (1980). "The Adsorption Force Theory of Frost Heaving." Cold Regions Science and Technology, Vol. 3, pp. 57-81.

Holtz, R.D. and Kovacs, W.D. (1981). An Introduction to Geotechnical Engineering. Englewood Cliffs NJ: Prentice-Hall.

Taber, S. (1929). "Frost heaving." Journal of Geology, 38: 303–317. In Historical perspectives in frost heave research. CRREL Special Report 91-23, U.S. Army Cold Regions Research and Engineering Laboratory, Hanover, N.H., pp. 29–35.

Casagrande, L. (1938). "Examination of the sub-soil of roads." In Proceedings of the 8th International Road Congress, The Hague, pp. 1–27.

Beskow, G. (1946). "Supplement: some results of Scandinavian soil frost research 1935–1946." In Soil freezing and frost heaving with special applications to roads and railroads. Swedish Geological Society, Series Cv, No. 375, Year Book 3. Translated byJ.O. Osterberg. CRREL Special Report 91-23, U.S. Army Corps of Engineers, Cold Regions Research and Engineering Laboratory, Hanover, N.H., pp. 161–169.

Rengmark, F. (1963). “Highway pavement design in frost areas in Sweden.” Highway Research Record 33, Pavement Design in Frost Areas II. Design Considerations, pp. 137–157.

Taivenen, O.A. (1963). “Preventive measure to reduce frost action on highways in Finland.” Highway Research Record 33, pp. 202–216.

Zhang, X. and Belmont, N.(2009). “Use of Mirafi Nylon Wicking Fabric to Help Prevent Frost Heaving in Alaska Pavement: 1st, 2nd, 3rd, 4th and 5th progress reports.” Progress reports to TENCATE GEOSYNTHETICS (North America).

Zhang, X. and Presler, W. (2012). “Use of H2Ri Wicking Fabric to Prevent Frost Boils in the Dalton Highway Beaver Slide Area, Alaska.” *Alaska University Transportation Center (AUTC)* Project Report, No. RR10.02 & 510020, August, 2012.

Lin, C. and Zhang, X. (2015). “Review of the Characterization of Geotextile Hydraulic Behavior.” *Innovative Materials and Design for Sustainable Transportation Infrastructure*, Selected Papers from the International Symposium. on Systematic Approaches to Environmental Sustainability in Transportation, Fairbanks, AK, August 2-5, 2015, pp. 213.

Genuchten, V. A Closed-Form Equation for Predicting the Hydraulic Conductivity of Unsaturated Soils. Soil Science Society of America Journal, Vol. 44, No. 5, 1980, pp. 892-898